Facies (2012) 58:389–414
DOI 10.1007/s10347-011-0281-1

ORIGINAL ARTICLE

Evolution of pelagic swells from hardground analysis (Bathonian–Oxfordian, Eastern External Subbetic, southern Spain)

Luis M. Nieto · Matías Reolid · José M. Molina · Pedro A. Ruiz-Ortiz · Juan Jiménez-Millán · Javier Rey

Received: 6 June 2011 / Accepted: 19 November 2011 / Published online: 10 December 2011

Abstract The Middle Bathonian to Middle Oxfordian interval in the Eastern External Subbetic (Betic Cordillera, SE Spain) is characterized by Ammonitico Rosso facies including various stratigraphic breaks. Five hardground-bounded units are recognized in relation to hiatuses in the ammonite record at the following stratigraphic boundaries: Hg1 (Lower–Middle Bathonian), Hg2 (Middle–Upper Bathonian), Hg3 (Lower–Middle Callovian), Hg4 (Middle–Upper Callovian), and Hg5 (Callovian–Oxfordian). Interesting features of these hardgrounds include their microfacies, ferruginous crusts and macro-oncoids, taphonomy of macroinvertebrates, trace fossils, neptunian dykes, and the hiatuses associated with each of them. The main hardgrounds (Hg1, Hg2, and Hg5) contain trace fossils of the *Cruziana* and *Trypanites* ichnofacies as well as abundant fossil macroinvertebrates with taphonomic features evidencing corrasion, early diagenesis, and reworking, indicating substrate evolution from softground to hardground. Neptunian dykes affected the trace fossils and ammonoid moulds, and their walls and the hardground surfaces were colonized by ferruginous microbial crusts. These features are characteristic of the External Subbetic pelagic swells, where the absence of sedimentation, sediment bypassing and erosion, and early diagenesis during relative sea-level falls produced hardgrounds. The neptunian dykes are indicative of tectonic activity in the areas of pelagic swells. Ferruginous crusts and macro-oncoids developed only on hardground surfaces and neptunian dykes walls prior to deposition of condensed bioclastic beds, which are interpreted as the first deposits after hardground development and are related to the onset of transgression. The varying ranges of the gaps as well as lateral facies changes are related to different local paleobathymetry controlled by the activity of listric faults.

Keywords Pelagic swells · Hardground · Stratigraphic break · Condensed section · Ichnofossil · Neptunian dyke · Bathonian–Oxfordian · Subbetic

L. M. Nieto (✉) · M. Reolid · J. M. Molina · P. A. Ruiz-Ortiz · J. Jiménez-Millán
Departamento de Geología,
Universidad de Jaén, 23071 Jaén, Spain
e-mail: lmnieto@ujaen.es

J. Rey
Departamento de Geología, EPS Linares,
Universidad de Jaén, 23700 Linares, Spain

Introduction

The Bathonian–Oxfordian transition in the western Tethys is characterized by discontinuous sedimentation in both epicontinental and epi-oceanic environments, marked by a complex succession of stratigraphic breaks. These sedimentary discontinuities are represented in several domains, for instance the Iberian Range (Aurell et al. 1994, 1999; Ramajo and Aurell 1997; Ramajo et al. 2002; Meléndez et al. 2005), the Côte D'Or (Courville and Collin 1997), Chaignay (Scouflaire et al. 1997), the western Subalpine Basin (Dromart 1989), the southeastern Paris Basin (Lorin et al. 2004; Collin et al. 2005), the Jura region of Switzerland (Gygi 1981; Huber et al. 1987), Swabia (Gygi and Persoz 1987), and the Maghreb (Soussi and M′rabet 1991; Kadiri 2002; Reolid et al. 2011). In the Betic External Zone, which represents the South Iberian Paleomargin during the Mesozoic, major stratigraphic gaps and discontinuity surfaces occur in the Bathonian–Oxfordian interval (Sequeiros 1974, 1979; Seyfried 1978; García-Hernández et al. 1980, 1989; Sandoval 1979, 1983; Molina 1987; Marques et al. 1991;

Martín-Algarra and Vera 1994; Vera and Martín-Algarra 1994; Martín-Algarra and Sánchez-Navas 2000; O'Dogherty et al. 2000; Vera 2001; Reolid et al. 2010).

The deposits studied herein, corresponding to the Bathonian–Oxfordian interval, are characterized by intense condensation and by stratigraphic breaks usually recorded as hardgrounds (Rey 1993; Nieto 1997). These deposits can be included in the upper part of the transgressive–regressive cycles T/R7 and T/R8 proposed by Jacquin and de Graciansky (1998) and Jacquin et al. (1998). The discontinuity at the base of cycle T/R8 is coeval to an important extensional event related to the rifting of the North Sea and the Tethys. In the Paris Basin, the maximum flooding event of T/R8 is represented by condensed beds with iron ooids separated by discontinuity surfaces interpreted as related to a deformation episode during the Late Callovian (Jacquin et al. 1998).

Cecca et al. (2005) and Rais et al. (2007) proposed a global reduction in carbonate paleoproductivity related to climatic and oceanographic changes during the Early Bathonian–Middle Oxfordian. Reduced carbonate accumulation during the Middle–Late Jurassic transition has been determined to be global, and explained by sea-level fall caused by global cooling during the Callovian–Oxfordian (Podhala et al. 1998; Dromart et al. 2003a, b). In this context, hardground formation in the Jura and Helvetian Domains resulted from significant oceanographic reorganization of the Western Tethys owing to the development of the so-called Hispanic Corridor (Rais et al. 2007). Other authors (Azeredo et al. 2002; Dromart et al. 2003a, b; Fürsich et al. 2005; Hautvelle et al. 2006) suggest climatic changes to explain the hardground origin.

According to Ziegler (1989), the Middle–Late Jurassic transition was an active tectonic period in which the tectonic setting changed from extensional (related to the expansion of the Central Atlantic) to transtensional (as a consequence of the sinistral movement of Africa–South America with respect to Laurasia). This led to the opening of new basins in the Western Tethys. In the Lusitanian Basin, Leinfelder (1993) and Azeredo et al. (2002) have associated the Callovian–Oxfordian discontinuity with the significant changes at the Mid-Atlantic Ridge.

The modification of the tectonic regime was also recognized at the South Iberian Paleomargin (Ruiz-Ortiz et al. 1997; O'Dogherty et al. 2000), where different discontinuities were identified (Lower–Middle Bathonian boundary, Middle–Upper Bathonian boundary, Lower–Middle Callovian boundary, Middle–Upper Callovian boundary and Callovian–Oxfordian boundary). These authors interpreted the intra-Bathonian discontinuities as related to significant paleogeographic changes in the South Iberian Paleomargin. Vera et al. (1984) and Molina (1987) interpreted the Upper Bathonian–Callovian stratigraphic discontinuity in the Western External Subbetic to be a consequence of the relative low sea level and of sinistral wrench faulting, which shifted the African Plate to the east. Vera (2001) indicated that the change from an extensional to a transtensional regime during the Callovian–Oxfordian boundary was related to the separation of the African Plate, the Iberian Plate, and the Mesomediterranean Microplate.

Fig. 1 **a** Location of the study region in the Iberian Peninsula. **b** Geological map of the eastern part of the Betic Cordillera. **c** Paleogeographic reconstruction of the South Iberian Paleomargin for the Late Kimmeridgian (after Vera 2001) **d** Geological map of the Quípar Unit. **e** Regional geological sketch of the easternmost zone of the study area (Lúgar–Corque, Cantón, Crevillente and Reclot, units) ▶

The aim of this research is to perform a detailed integrated analysis of hardgrounds, condensed levels, and related features in the Lower Bathonian to Lower Oxfordian part of the Ammonitico Rosso Formation of the Eastern External Subbetic (Fig. 1a, b). Hardgrounds and condensed beds that formed there represent different stages in the tectono-sedimentary evolution of the pelagic swells. This study focuses on expanding our knowledge about (1) sedimentary and tectonic processes that occurred during the hiatus associated with each discontinuity, (2) hardground evolution from the initial stages of stratigraphic omission to renewed onset of sedimentation, and (3) control mechanisms for the beginning of sedimentation. To achieve these goals, sedimentological, taphonomic, ichnological, mineralogical, and geochemical aspects were taken into account.

Geological setting

The studied outcrops are located in the provinces of Alicante and Murcia (SE Spain), which paleogeographically belong to the South Iberian Paleomargin (Fig. 1a, b, c). These outcrops are located in five different tectonic units: Quípar (Quípar section), Lúgar–Corque (Lúgar 62-1, Lúgar 62-2, and Caprés sections), Cantón (Boquera-43 section), Crevillente (Sanyuri-35C and San Cayetano-36 sections), and Reclot (Rambla Honda-1 and Rambla Honda-2 sections) (Fig. 1d, e).

The stratigraphic sequences of the tectonic units (Fig. 2a) are characterized by Hettangian to Lower Pliensbachian shallow carbonate platform dolostones and limestones (Gavilán Formation) followed by Upper Pliensbachian–Toarcian pelagic and hemipelagic marl-limestone rhythmites (Zegrí Formation), Aalenian–Bajocian cherty limestones (Veleta Formation), and Bathonian to Berriasian nodular limestones (Upper Ammonitico Rosso Formation, Fig. 2b, c). Consequently, in the Middle to Late Jurassic (Fig. 1c), the breakup of the earliest Jurassic epeiric carbonate platform transformed the Eastern External Subbetic into an epioceanic

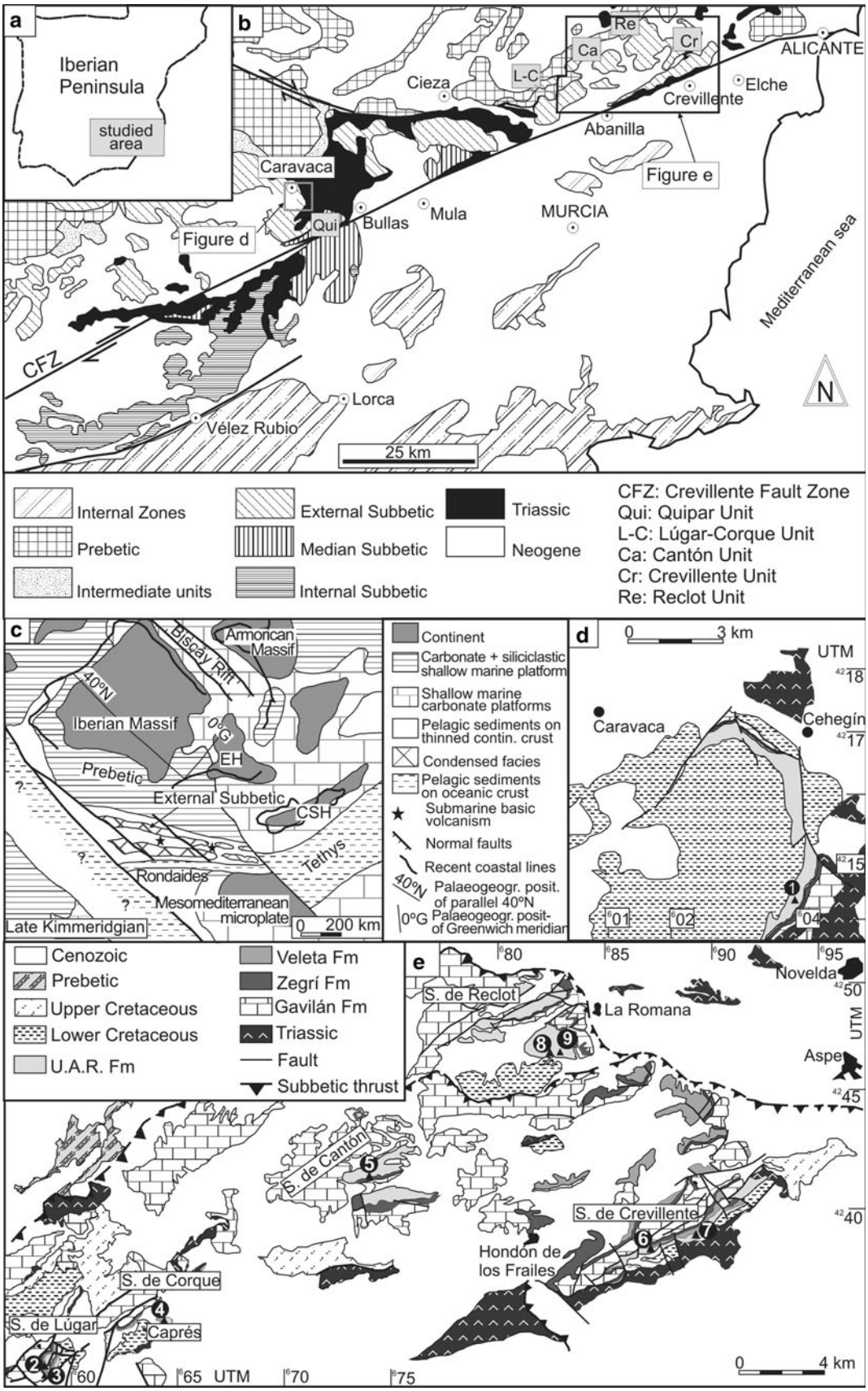
a
Iberian Peninsula
studied area
b
Re
Ca
Cr
ALICANTE
Cieza
L-C
Elche
Crevillente
Abanilla
Figure e
Caravaca
Qui
Bullas
Mula
MURCIA
Figure d
Mediterranean sea
CFZ
Lorca
Vélez Rubio
25 km
N
Internal Zones
Prebetic
Intermediate units
External Subbetic
Median Subbetic
Internal Subbetic
Triassic
Neogene
CFZ: Crevillente Fault Zone
Qui: Quipar Unit
L-C: Lúgar-Corque Unit
Ca: Cantón Unit
Cr: Crevillente Unit
Re: Reclot Unit
c
Armoican Massif
Biscay Rift
40ºN
Iberian Massif
0ºG
EH
Prebetic
External Subbetic
CSH
Tethys
Rondaides
Mesomediterranean microplate
Late Kimmeridgian
0 200 km
Continent
Carbonate + siliciclastic shallow marine platform
Shallow marine carbonate platforms
Pelagic sediments on thinned contin. crust
Condensed facies
Pelagic sediments on oceanic crust
Submarine basic volcanism
Normal faults
Recent coastal lines
Palaeogeogr. posit. of parallel 40ºN
Palaeogeogr. posit. of Greenwich meridian
d
0 3 km
UTM
Caravaca
Cehegín
Cenozoic
Prebetic
Upper Cretaceous
Lower Cretaceous
U.A.R. Fm
Veleta Fm
Zegrí Fm
Gavilán Fm
Triassic
Fault
Subbetic thrust
e
S. de Reclot
La Romana
Novelda
Aspe
S. de Cantón
S. de Crevillente
Hondón de los Frailes
S. de Corque
S. de Lúgar
Caprés
UTM
0 4 km

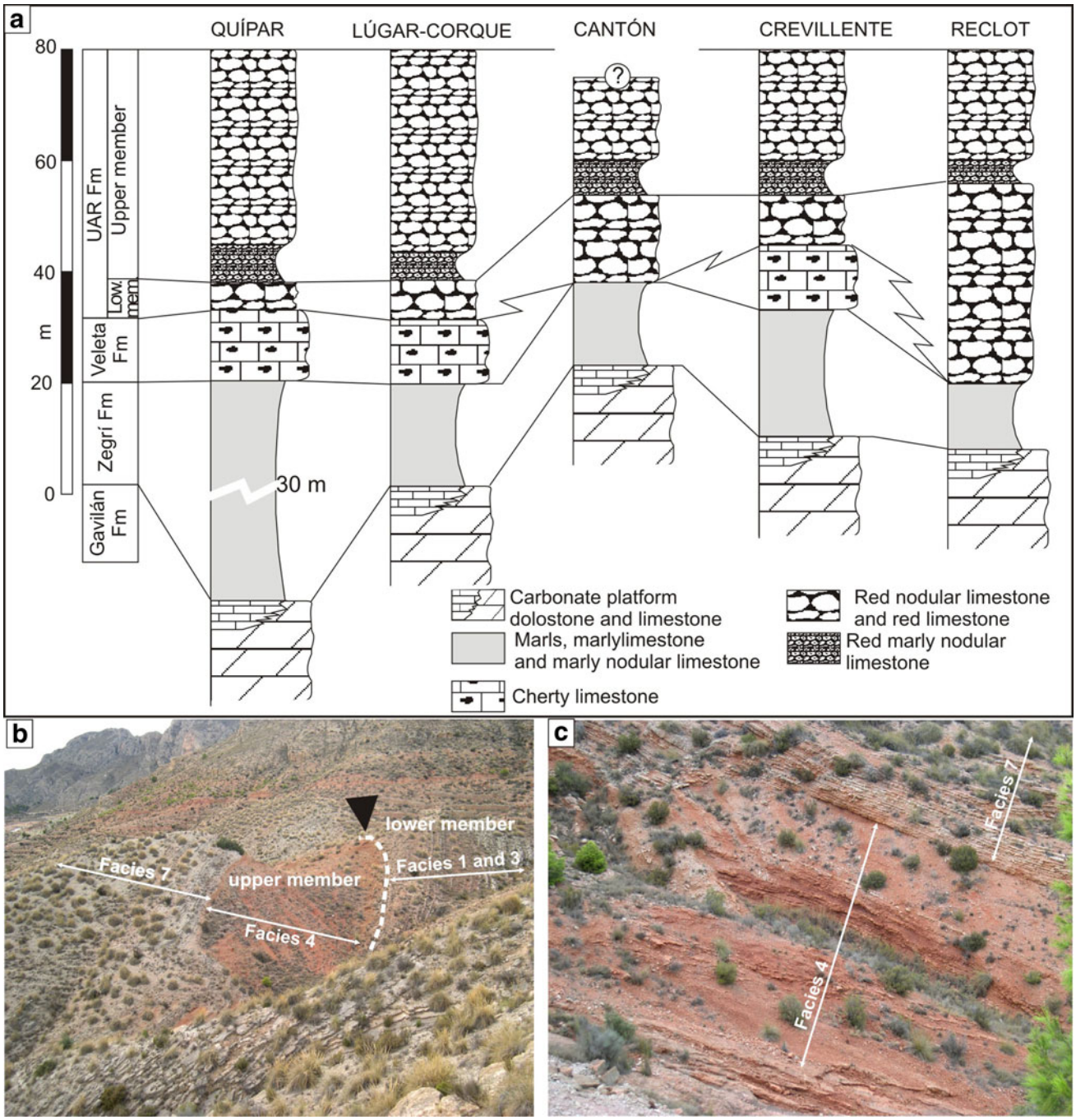

Fig. 2 **a** Synthetic Jurassic stratigraphic sections of each tectonic unit studied. **b** Panoramic view of the UAR Formation in the Lúgar–Corque Unit. **c** Field aspect of the upper member of the UAR Formation in the Lúgar–Corque Unit

pelagic swell area bounded by listric faults (Molina et al. 1999; Vera 2001; Vera et al. 2004).

Two members, lower and upper, are differentiated within the Upper Ammonitico Rosso Formation (UAR) on the base of the presence of stratigraphic discontinuity surfaces (paraconformities and local disconformities associated with neptunian dykes) and condensed sediments in the Bathonian–Oxfordian part of the stratigraphic succession. Seven lithofacies have been distinguished within this stratigraphic interval, which are discussed in detail below (Table 1 and Figs. 3, 4, 5). Previous studies on Fe–Mn-rich and P-rich microbial structures related to the hardgrounds in some of the sections analyzed and in other areas of the Subbetic Domain were performed by Vera and Martín-Algarra (1994) and Martín-Algarra and Sánchez-Navas (2000).

Table 1 Facies recognized in the studied stratigraphic sections

No of facies	Lithofacies	Description	Biota	Other allochems
Facies 1	Massive red limestone	Beds 0.8–1.4 m thick. Parallel lamination and hummocky cross stratification. Microfacies: mudstone, wackestone, or "filament" packstone	"Filaments" (*Bositra buchi*), *Protopeneroplis striata*, *Globuligerina* sp., crinoids, radiolarians, sponge spicules	Peloids Micritic extraclasts
Facies 2	Bioclastic limestone	Mean thickness of beds 30 cm. Massive, without lamination. Microfacies: bioclastic packstone	Brachiopods, bivalves, echinoderms, *Globuligerina* sp., *Protopeneroplis striata*, *Valvulina lugeoni*	Peloids
Facies 3	Compact red nodular limestone	Thickness of beds 10–20 cm. Microfacies: mudstone and radiolaria wackestone	Radiolarians, ammonites, Aptychus, gastropods, brachiopods, sponge spicules	Bioclasts
Facies 4	Nodular red marly limestone	Beds 3–30 cm thick. Microfacies: *Globuligerina* mudstone/wackestone, sponge spicules mudstone, and radiolarian wackestone	*Globuligerina* sp., sponge spicules, radiolaria	Peloids Bioclasts
Facies 5	Red limestone without nodular features	Beds 5–10 cm thick. Massive, without lamination. Microfacies: *Globuligerina* wackestone/packstone	*Globuligerina* sp. Radiolarians, sponge spicules, ammonites, belemnites, Aptychus	Peloids
Facies 6	Conglomerate	Clast-supported. Some clasts exhibiting plastic deformation. Others are ammonites. Beds 30–70 cm thick. Microfacies of clasts: *Saccocoma* mudstone/wackestone and radiolarian mudstone/wackestone	Fragmented ammonoids and belemnites, *Globuligerina* sp. and crinoids (*Saccocoma* sp.)	Peloids and lumps
Facies 7	Nodular pink limestone	Beds between 5 and 20 cm thick. Bioturbation important (*Thalassinoides*, *Planolites*, *Chondrites*). Microfacies: *Saccocoma* mudstone/wackestone and radiolarian mudstone/wackestone	Unclassified bioclasts	Peloids

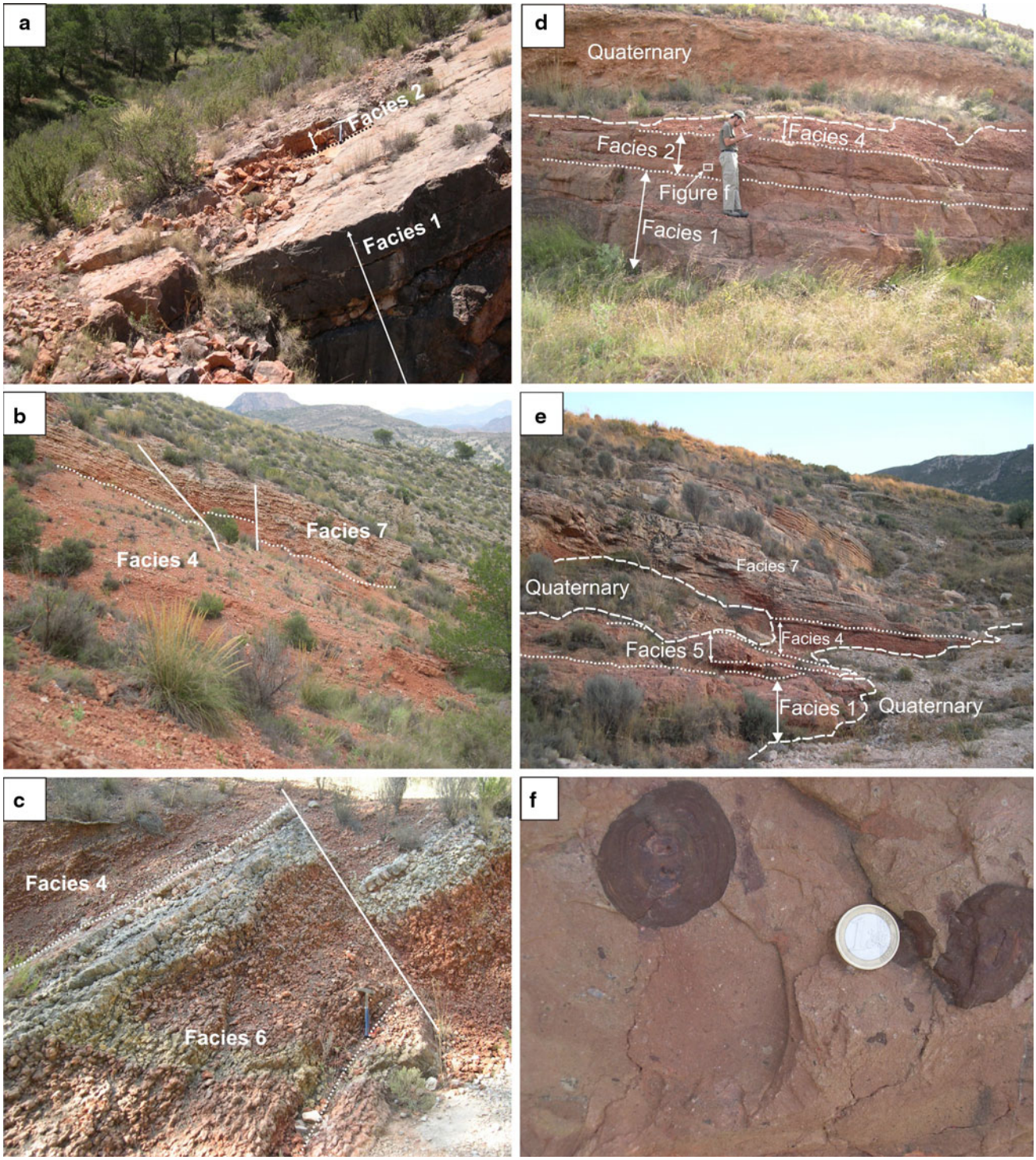

Fig. 3 Outcrop views of the different facies in some studied sections. **a** Lúgar 62-1. **b** Lúgar 62-2. **c** Sanyuri 35C. **d** Rambla Honda-1. **e** Rambla Honda-2. **f** Detail of facies 2 (bioclastic limestone) in the Rambla Honda-1 section

Lower member of the UAR Formation

This member (Middle Jurassic in age) is made up of nodular red limestones (facies 1 in Table 1; Figs. 2b, 3, 4a). Incipient hardgrounds are observed at the top of some beds. The microfacies are wackestones-packstones with filaments (*Bositra buchi*), peloids, sponge spicules, crinoids, radiolaria, foraminifera (*Protopeneroplis striata*, *Globuligerina* sp.) and indeterminate bioclasts. A hardground rich in trace fossils tops this member (Fig. 3a).

In some stratigraphic sections (e.g., Quípar, Lúgar 62-1, Caprés, San Cayetano-36, and Rambla Honda-1; Figs 3a, d,

e, f, 5), above the hardground there is a bioclastic bed, up to 70 cm thick, that quickly pinches out (facies 2 in Table 1, Figs. 3a, d, f, 4b). This bed is a bio-packstone with filaments (*Bositra buchi*), crinoids, and *Globuligerina* sp., and it commonly includes Fe-rich macro-oncoids (Fig. 3f). At the top of this bed, there is another hardground with a ferruginous crust (2–3 cm thick), ammonoid moulds (*Procerites* and *Wagnericeras*), and trace fossils (*Thalassinoides*). Both hardgrounds are commonly superimposed when the bioclastic bed is not present.

Rey (1993) and Nieto (1997) considered the top of the lower member as a diachronous surface, Early Bathonian in age (*Zigzagiceras zigzag* Biozone, Figs. 6, 7), in the Reclot and Cantón units and in some sections of the Lúgar–Corque Unit, and Middle Bathonian in the Crevillente and Quípar units, and locally in the Lúgar–Corque Unit (Figs. 6, 7).

Upper member of the UAR Formation

This member, Callovian–Berriasian in age, has a lower part of alternating compact red nodular limestone (facies 3, mudstones and radiolarian wackestones, Table 1, Fig. 4c, d), and red nodular marly limestone (mudstones and wackestones containing *Globuligerina* sp, facies 4, Table 1; Figs. 2b, c, 3b, c, d, e, 4e), including beds of red limestone without evident nodular structure (facies 5 in Table 1, and Figs. 3e, 4f, 5). Its upper part is a pink nodular limestone (mudstones and wackestones with *Saccocoma*, facies 7, Table 1; Figs. 2b, c, 3e, 4h, 5). In the Crevillente sections, a clast-rich bed is located at the base of the lowermost (Callovian) part of this upper member in the same stratigraphic position (facies 6 in Table 1, and Figs. 3c, 4g, 5).

The base of the upper member is also a diachronous surface dated as Late Oxfordian (*Dichotomoceras bifurcatus* Biozone, Figs. 6, 7) in the Cantón, Crevillente and Reclot units as well as in some sections of the Lúgar–Corque Unit (Figs. 5, 7). In the Caprés section (Figs. 5, 7), this surface has been dated as Early Oxfordian (Checa and Sequeiros 1990), whereas in the Quípar Unit the first sediments of this member have been dated as Middle Oxfordian (Rey 1993; Figs. 5, 7). In this paper we also report Callovian beds in the boundary zone between the lower and upper members of the UAR Formation.

Methods

Nine sections representative of the five tectonic units of the Eastern External Subbetic have been studied (Figs. 1, 2, 3, 4, 5). Field observations were complemented with detailed sampling focused on the microfacies analysis of polished and thin-sections using binocular magnification glass and the petrographic microscope. A detailed biostratigraphy was obtained from the study of 155 ammonoid moulds by using the ammonoid biozonation for the Bathonian, Callovian, and Oxfordian of the Betic Cordillera by various authors (Sequeiros 1974, 1979; Olóriz 1978, 1979; Sandoval 1979, 1983; Sequeiros and Olóriz 1979; Caracuel 1996). This biozonation (Fig. 6) has been correlated with the sub-Mediterranean biozones proposed by Ogg (2004). The chronostratigraphic diagram in Fig. 7 was developed on the basis of this correlation.

Only neptunian dykes perpendicular to bedding, and therefore originally subvertical, were considered. The original strike of the dykes was recorded in different hardgrounds after restoring the hardground surfaces to the horizontal (i.e., after correcting for tilting). The rotation of the tectonic units during the Alpine Orogeny is also considered in accordance to the data of Platzman and Lowrie (1992) and Platt et al. (2003). The first authors estimated that the mean clockwise vertical axis rotation for the Subbetic was 60°. Platt et al. (2003) calculated the vertical axis rotation for different tectonic units belonging to the Eastern External Subbetic. For the purposes of our research, the data relative to the Quípar Unit was taken (54° of the clockwise vertical axis rotation).

Petrographic microscopy was used to determine the rock textures from thin- sections, including those of Fe–Mn crusts and macro-oncoids. Analysis of the Fe–Mn encrustations focused on the lamination, coating thickness, microbial fabrics and mineralogy. A SCI Quanta 400 instrument from the Centro Andaluz de Medio Ambiente (CEAMA) was used to obtain high-resolution scanning electron microscopy photographs. The mineral composition of the Fe–Mn crusts was determined by X-ray diffraction (XRD) using a Siemens D-5000 diffractometer at the Centro de Instrumentación Científica of the University of Jaén. In addition, thin-sections and Fe–Mn crust fragments were gold- and carbon-coated, and examined directly under the scanning electron microscope (SEM) using secondary electrons, back-scattered electron (BSE) imaging, and energy-dispersive X-ray (EDX) analyses to study their internal ultrastructure, crystal morphology, and geochemical composition, by using a Zeiss DSM 950 SEM at the Centro de Instrumentación Científica (CIC) of the University of Granada.

Taphonomic analysis of macroinvertebrates was performed on the most favorable hardground surfaces (Lower–Middle Bathonian, Middle–Upper Bathonian, and Callovian–Oxfordian discontinuities) in the Reclot, Lúgar–Corque, and Quípar tectonic units. The following taphonomic features were taken into account for more than 250 remains of fossil macroinvertebrates: (1) size, (2) position within the bed, (3) orientation, (4) type of preservation (shell preservation and sedimentary infill), (5) corrasion (sensu Brett and Baird 1986), (6) fragmentation, and (7) biogenic

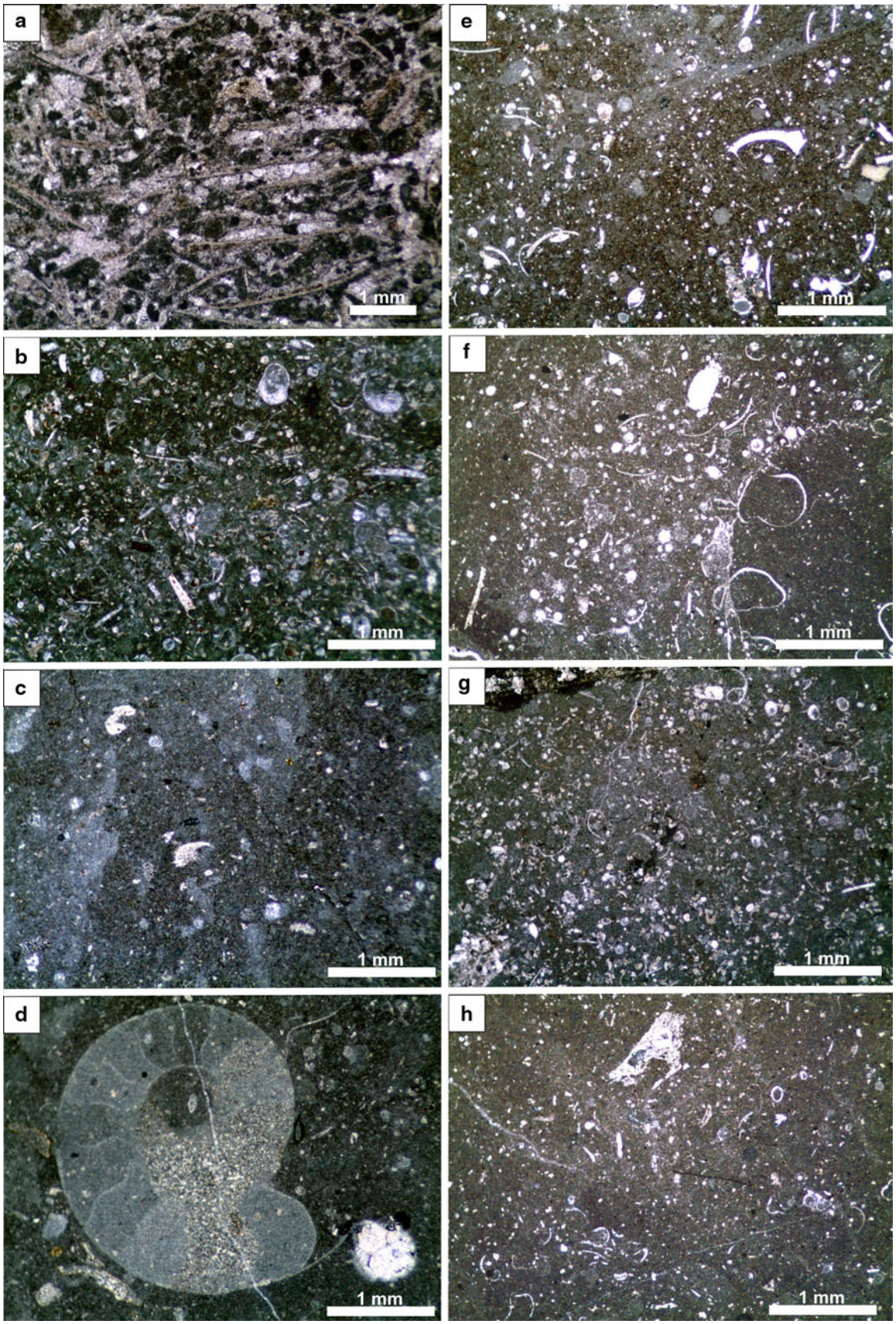
a
1 mm
e
1 mm
b
1 mm
f
1 mm
c
1 mm
g
1 mm
d
1 mm
h
1 mm

◀ **Fig. 4** Textural features of the facies considered in Table 1. **a** Facies 1: Wackestone to packstone of "filaments" (*Bositra buchi*). **b** Facies 2: Bioclastic packstone with *Globuligerina* sp. **c** Facies 3: Mudstone. **d** Facies 3: Ammonoid embryo. **e** Wackestone with radiolarian and other bioclasts. **f** Facies 5: Wackestone to packstone of *Globuligerina* sp. **g** Facies 6: Radiolarian wackestone. **h** Facies 7: *Saccocoma* wackestone

encrustation. The analysis of fragmentation, corrasion, and encrustation was undertaken using the fragmentation index (F_i), corrasion index (C_i), and encrustation index (E_i) proposed by Olóriz et al. (2002, 2004).

Facies distribution

Quípar unit

The Quípar section (Fig. 5) is characterized by compact red nodular limestones (facies 3, Table 1; Fig. 4c, d) of Middle Bathonian age (lower member of the UAR Fm., column 1 in Figs. 1, 7). The top of these deposits is a hardground (Hg2 in column 1 of Figs. 5, 7) with abundant ammonoids, belemnites, and ferruginous macro-oncoids. In addition, various families of neptunian dykes have been detected. Next in the section there are some dm-thick bioclastic beds (3–40 cm) with hardgrounds at the top (Hg2 and 3 in column 1 of Fig. 7) and common trace fossils and ferruginous crusts, which contain Callovian ammonoids. Middle to Upper Oxfordian red nodular marly limestone forms the base of the upper member of the UAR Formation.

Lúgar–Corque unit

Three sections have been selected from this tectonic unit: Lúgar 62-1, Lúgar 62-2 and Caprés (Fig. 5).

In the Lúgar 62-1 section the Lower–Middle Bathonian massive red limestones (facies 1 in Table 1, Figs. 3a, 4a) are topped by a hardground with neptunian dykes and abundant ammonoids (Hg1 + 2 in column 2 of Figs. 5, 7). One bioclastic bed (facies 2, Table 1, Fig. 3a) overlies this hardground and contains ferruginous macro-oncoids. The top of this bioclastic bed is another hardground with ferruginous crusts, trace fossils, ammonoids, and belemnites (Hg5 in column 2 of Figs. 5, 7). Up-section there are red nodular marly limestones (facies 4, Table 1, Fig. 4e) of the upper member, with ammonoids recording an Oxfordian age.

The Lúgar 62-2 is very close to the Lúgar 62-1 section, but the bioclastic bed is not present there. The top of the Lower–Middle Bathonian massive red limestones is a hardground with ammonoids, belemnites, trace fossils, and neptunian dykes (Hg1–5 in column 3 of Figs. 5, 7), all covered with ferruginous crusts and macro-oncoids with cores formed by ammonoids and belemnites. Upper Oxfordian red nodular marly limestones (Figs. 2c, 3b) cover the stratigraphic break.

In the Caprés section (Figs. 2b, 5), the Lower to Middle Bathonian massive limestones of the lower member (facies 1, Table 1) are terminated by a hardground with ammonoids, belemnites, and ferruginous macro-oncoids at the top (Hg2 in Figs. 5, 7, column 4). Above this hardground, there is a 60-cm-thick stratigraphic interval of red nodular marly limestone (facies 4, Table 1, Fig. 4e), with some incipient hardgrounds and thin ferruginous crusts capping the top of several beds. In these levels, Checa and Sequeiros (1990) found abundant Callovian ammonoids. Nodular marly limestones with Lower, Middle and Upper Oxfordian ammonoids (Checa and Sequeiros 1990) overlie these rocks.

Cantón unit

Only the Boquera-43 section from this unit has been analyzed (Figs. 1e, 5). A hardground with trace fossils, ammonoid moulds, and neptunian dykes (Hg1–5 in Figs. 5, 7, column 5) is observed at the top of Lower Bathonian massive red limestones (facies 1, Table 1, Fig. 4a). Ferruginous crusts and macro-oncoids are common on this surface. The sedimentation continues with nodular red marly limestones with *Dichotomoceras bifurcatus* and *Gregoryceras fouquei*, typical Late Oxfordian ammonoids (facies 4, Table 1, Fig. 4e).

Crevillente unit

In this tectonic unit, two sections are representative of the Middle–Upper Jurassic interval: Sanyuri-35C and San Cayetano-36 (columns 6 and 7 in Figs. 5, 7).

In the Sanyuri-35C section, there is a hardground (Hg2 in Figs. 5, 7, column 6) on top of Middle Bathonian massive red limestones (facies 1, Table 1). It is followed by a 75-cm-thick conglomerate interval (facies 6, Table 1, Figs. 3c, 4g) with moulds of reworked Callovian ammonoids (*Choffatia* sp. and *Reineckeia* sp.). The conglomerate is separated from the overlying red nodular marly limestones (facies 4, Table 1, Figs. 3c, 4e) by an omission surface (laterally an incipient hardground: Hg5 in Figs. 5, 7, column 7) without oxyhydroxide crusts and macro-oncoids or other features typical of the well-developed hardgrounds.

In the San Cayetano-36 section, the transition from the massive red limestones of the lower member (Lower Bathonian) to the upper member is represented by a hardground (Hg1 in Figs. 5, 7, column 7) followed by a 50-cm-thick Middle Bathonian limestone topped by a second hardground with trace fossils and a thin ferruginous crust (Hg2 in Figs. 5, 7, column 7). The Hg2 hardground is overlain by nodular red marly limestones (facies 4,

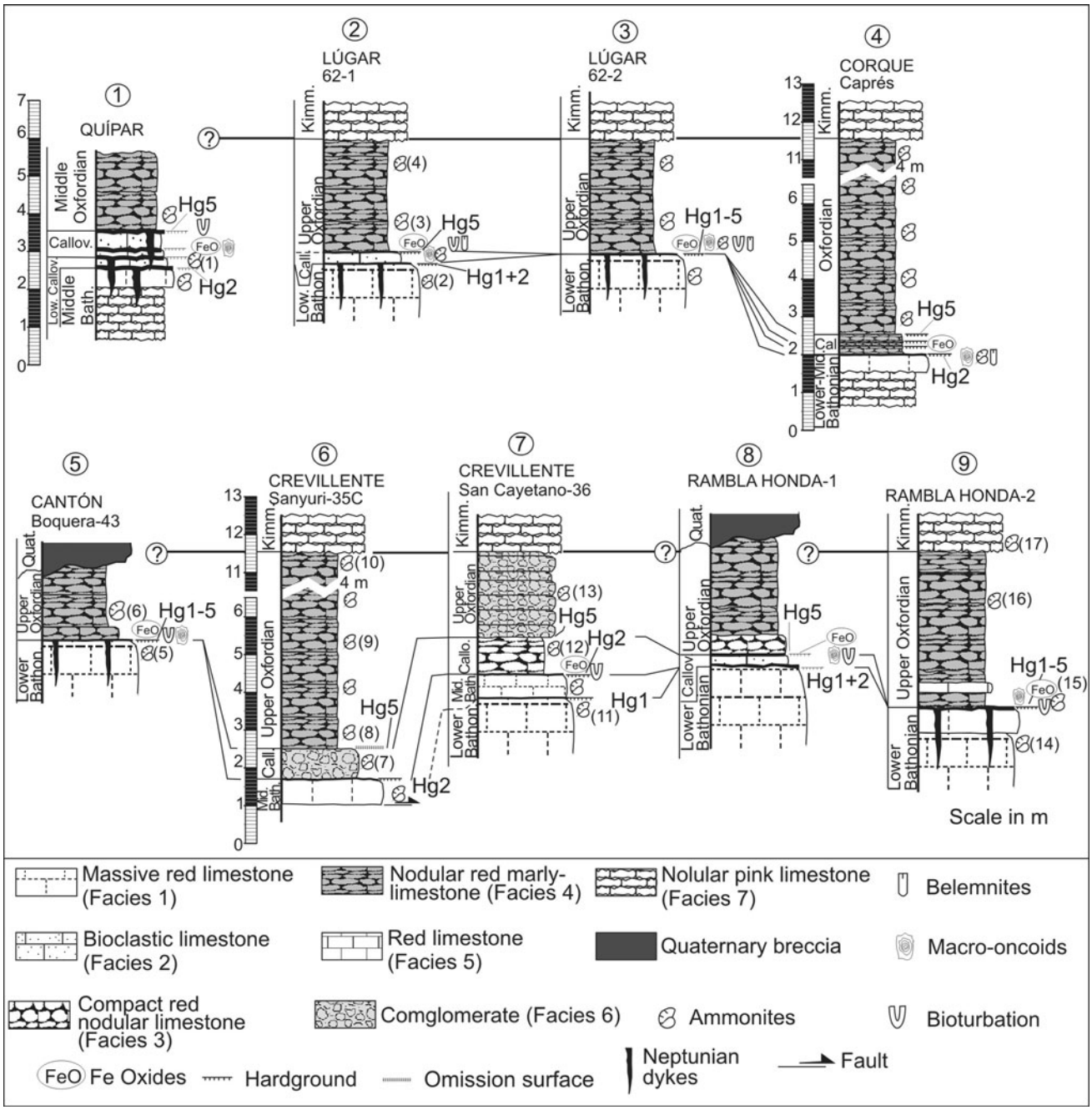

Fig. 5 Detailed stratigraphic sections of the studied successions. Key for fossil content (number in brackets denote classified ammonite levels): (1) *Choffatia* sp., *Indosphinctes* sp., *Macrocephalites* sp.; (2) *Morphoceras patescens*; (3) *Dichotomosphinctes* sp., *Orthosphinctes* sp., *Discosphinctes* sp., *Epipeltoceras* sp.; (4) *Orthosphinctes* sp.; (5) *Procerites* sp., *Nannolytoceras tripartitum;* (6) *Dichotomoceras bifurcatum*, *Gregoryceras fouquei*, *Sowerbyceras tortisulcatum*; (7) *Choffatia* sp., *Reineckeia* sp.; (8) *Dichotomoceras bifurcatum*, *Dichotomosphinctes* sp.; (9) *Euaspidoceras* sp.; (10) *Epipeltoceras bimammatum*; (11) *Cadomites bremeri*; (12) *Choffatia* sp.; (13) *Sowerbyceras tortisulcatum*, *Dichotomoceras bifurcatum*, *Dichotomosphinctes* sp., *Epipeltoceras* sp., ammonites mixed; (14) *Nannolytoceras tripartitum*; (15) *Holcophylloceras* sp., *Dichotomoceras bifurcatum*, *Dichotomosphinctes* sp.; (16) *Epipeltoceras* sp., *Sowerbyceras tortisulcatum*; (17) *Mesosimoceras* sp

Table 1, Fig. 4e) containing *Choffatia* sp., a Callovian ammonite. Next in the section are conglomerates, 2.5 m thick (facies 6, Table 1, Fig. 4g), with the Upper Oxfordian ammonites *Dichotomoceras bifurcatus* and *Epipeltoceras bimammatum*.

Reclot unit

Two sections have been selected as representative of this time interval in the Reclot Unit: Rambla Honda-1 and Rambla Honda-2 (Figs. 5, 7).

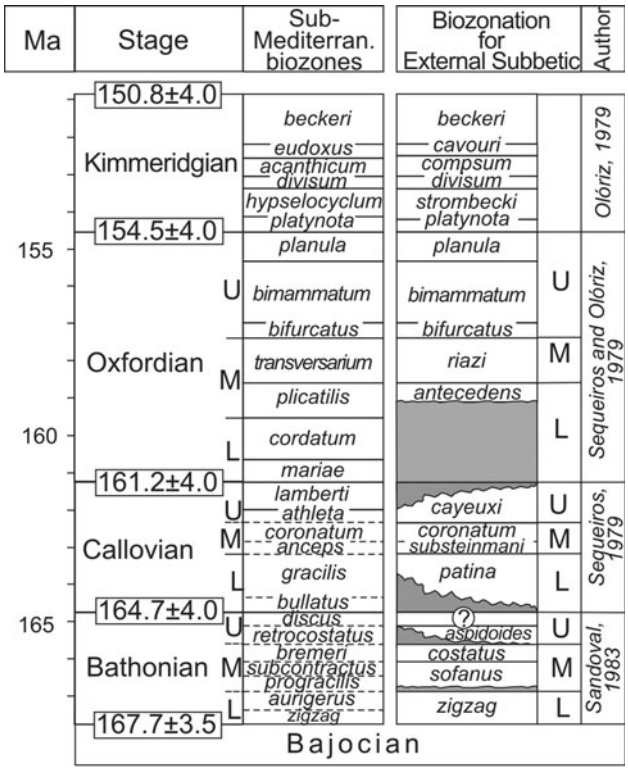

Fig. 6 Correlation between the biozonation proposed for the External Subbetic Zone and that proposed by Ogg (2004) for the Submediterranean domain. Geochronometry according to the same author

In the first section (Rambla Honda-1, column 8 in Figs. 5, 7), Lower Bathonian red massive limestones (facies 1, Table 1, Figs. 3d, 4a) are topped by a hardground (Hg1 + 2 in Figs. 3d, 5), followed by a 50-cm-thick Callovian bioclastic bed (facies 2, Table 1, Figs. 3d, f, 4b). The top of this bioclastic bed is a second hardground, attributed to the Hg5 (Figs. 5, 7, column 8), if it is supposed that the bioclastic bed represented the Callovian stage. This hardground contains trace fossils, ferruginous crusts (0.5–1 cm thick), and Fe-rich macro-oncoids, with a mean size near 40 mm. Upper Oxfordian compact red nodular limestones, corresponding to the base of the upper member of the UAR Formation (facies 3, Table 1, Figs. 3d, 4c, d, 8a), lie directly on this hardground.

The Rambla Honda-2 section (Fig. 5) is represented by Lower Bathonian massive red limestones (facies 1, Table 1, Figs. 3e, 4a), the top of which is defined by a hardground (Hg1–5 in Sect. 9 of Fig. 5) with abundant trace fossils (Fig. 8b, c) and large ammonoid moulds, and by neptunian dykes (Fig. 8c). These features are covered by Fe–Mn oxyhydroxide crusts and macro-oncoids (Fig. 8d). Above this hardground, red nodular marly limestones (facies 4, Table 1) with some levels made up by non-nodular red limestone (facies 5 in Table 1, Fig. 3e) are present in this section.

Chronostratigraphy and age of stratigraphic breaks

The top of the UAR Formation lower member is a diachronous surface. In the Reclot and Cantón units, and partially in the Lúgar–Corque Unit (Fig. 7), this surface postdates the Lower Bathonian (*Zigzagiceras zigzag* Biozone), whereas in the Crevillente and Quípar units, and locally in the Lúgar–Corque Unit, the recorded age below it is Middle Bathonian (top of the *Bullatimorphites costatus* Biozone, Fig. 7). In addition, the bottom of the UAR Formation upper member is also diachronous and dated as Late Oxfordian (*Dichotomoceras bifurcatus* Biozone, Fig. 7) in most sections, whereas Checa and Sequeiros (1990) reported Early Oxfordian ammonoids in the Caprés section (column 4 in Fig. 7). In the Quípar section, the base of the upper member is Middle Oxfordian (*Gregoryceras riazi* Biozone, Fig. 7). The time interval between the lower and upper members of the UAR Formation is not recorded in some cases, or is partially recorded by condensed bioclastic beds (locally conglomerates, Sanyurí-35C section, column 6 in Figs. 5, 7) with hardgrounds (Fig. 7).

In the Bathonian–Oxfordian interval, there are five stratigraphic breaks, usually identified as hardgrounds, within the UAR Formation (Fig. 7). They are dated as follows: Hg1 as the top of the *Zigzagiceras zigzag* Biozone, Lower–Middle Bathonian boundary; Hg2 as the top of the *Bullatimorphites costatus* Biozone, Middle–Upper Bathonian boundary; Hg3 as the Lower–Middle Callovian boundary (according to Checa and Sequeiros 1990); Hg4 as the Middle–Upper Callovian boundary; and Hg5 as the Callovian–Oxfordian boundary. The Hg1, Hg2, and Hg5 breaks have been identified in most outcrops of the Eastern and the Western External Subbetics and were reported as regional stratigraphic features of the External Subbetic successions by Ruiz-Ortiz et al. (1997). In contrast, Hg3 and Hg4 are only recorded in the westernmost units, Quípar and Lúgar–Corque, and are therefore considered as local features of the Eastern External Subbetic.

The hiatus associated with each unconformity varies according to the tectonic unit and, occasionally, even between outcrops of the same tectonic unit (Fig. 7). In some sections (Lúgar 62-2, Boquera, and Rambla Honda-2; Figs. 5, 7), there are Upper Oxfordian red nodular marly limestones (facies 4) above the hardground (Hg1) at the top of the massive red nodular limestones (facies 1). The hiatus associated with this discontinuity surface (Hg1) resulted from the superposition of all the stratigraphic lacunae related to the different hardground surfaces (from Hg1 to Hg5), and it is therefore the longest break (Middle Bathonian–Middle Oxfordian, *Gregoryceras riazi* Biozone; Fig. 7). According to the biostratigraphic data, the shortest hiatus probably covers the *Oxycerites aspidoides* Biozone

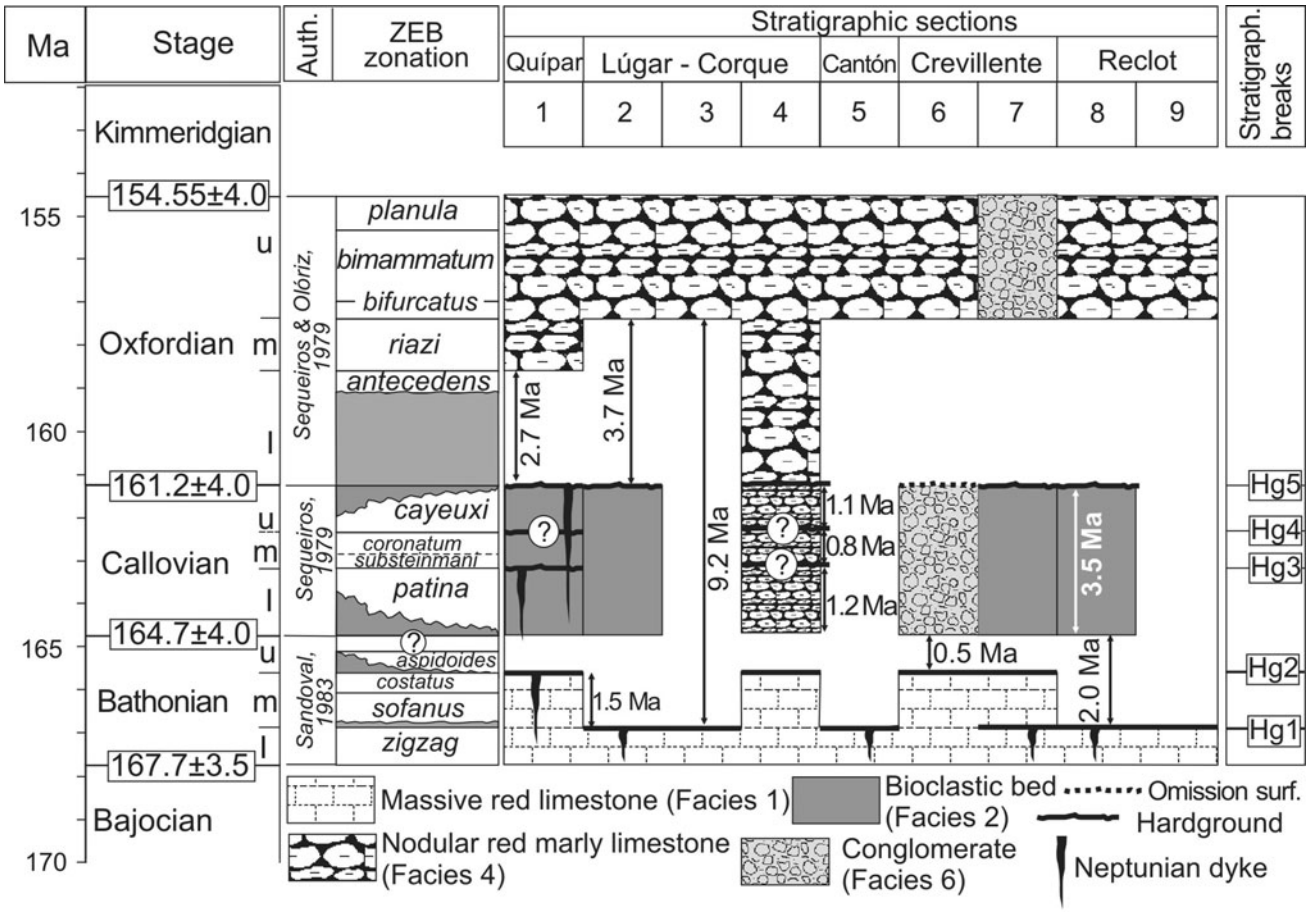

Fig. 7 Chronostratigraphic sketch of the studied sections indicating the location of the stratigraphic breaks and associated hiatuses. Geochronology according to Fig. 6. 1: Quípar; 2: Lúgar 62-1; 3: Lúgar 62-2; 4: Caprés; 5: Boquera-43; 6: Sanyuri-35C; 7: San Cayetano-36; 8: Rambla Honda-1; 9: Rambla Honda-2

(∼0.5 Ma), recorded in the Quípar and Caprés sections and both columns of the Crevillente unit (Fig. 7).

Sedimentological, taphonomic, and ichnological features related to hardgrounds

Ferruginous crusts and macro-oncoids

Hardgrounds Hg1, Hg2, and Hg5 are associated with abundant crusts and macro-oncoids composed of Fe–Mn oxyhydroxides (Jiménez-Millán and Nieto 2008). The macro-oncoids (mean size of 43 mm; range: 10–108 mm) consist of a core (molluscan fragments, indeterminate fossils or pelagic limestone clasts) coated by concentric laminae usually less than 30 mm thick (Fig. 9a).

The ferruginous encrustations show laminated fabrics made of alternating clear and dark laminae (20–140 μm thick) with planar, undulose (Fig. 9b) and arborescent morphologies (Fig. 9c, d; Reolid and Nieto 2010). The mineral association of both the ferruginous macro-oncoids and crusts is composed of goethite, calcite, lithiophorite, and cryptomelane (Jiménez-Espinosa et al. 1997; Martín-Algarra and Sánchez-Navas 2000; Jiménez-Millán and Nieto 2008). The Fe_2O_3 content is three to nine times higher than in the European Shale Composite of Haskin and Haskin (1966). The Mn content is always under 20% and the Fe/Mn ratio is usually less than 50. These crusts are enriched in Co, Ni, As, and Sb, whereas the REE content is close to that of the Recent hydrogenous Fe–Mn crusts. These crusts have a positive Ce anomaly (Jiménez-Millán and Nieto 2008; see also Martín-Algarra and Sánchez-Navas 1995).

Thin-section analysis reveals ovoid microspheres (40 μm in diameter) and filamentous microstructures (8 μm in diameter), occasionally with a trichomal microsphere arrangement. SEM analysis of the crust revealed three types of microbial structures (Reolid and Nieto 2010): (a) ovoid to sub-spherical forms (∼2 μm), interpreted as cyanobacteria coccoids, (b) straight to slightly curved cylindrical filaments (2–3.5 μm in diameter and >0.7 mm in length) with irregular branching, assigned to fungal hyphae, and

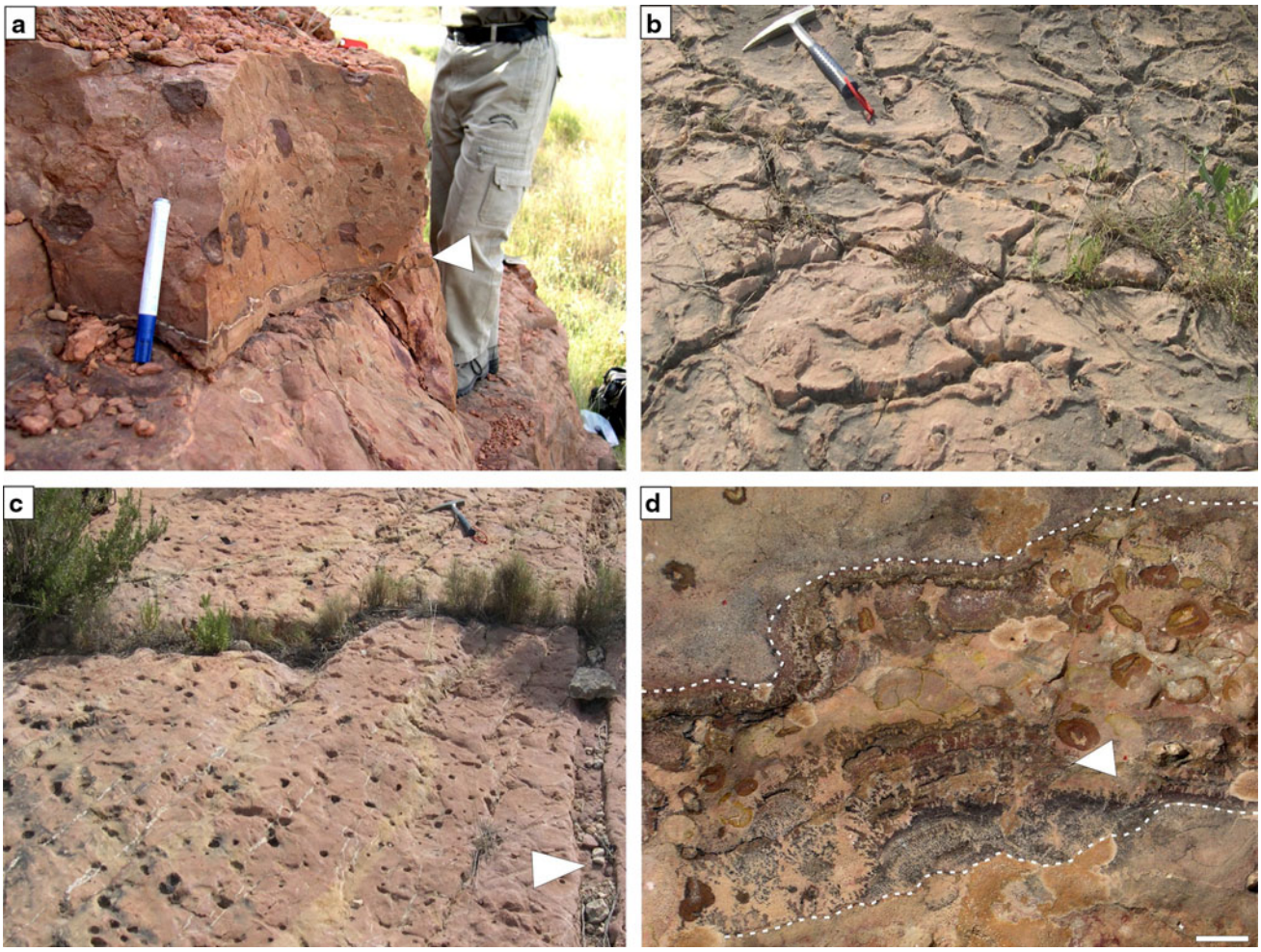

Fig. 8 Field aspects of the outcrops. **a** Bioclastic bed with ferruginous macrooncoids just above Hg1 (*white arrow*) in the Rambla Honda-1 section. **b** *Thalassinoides* from Hg1 in the Rambla Honda-2 section. **c** Borings and a neptunian dyke (*arrow*) from Hg1 in the Rambla Honda-2 section. **d** Ferruginous crust growing on the walls of neptunian dykes (endostromatolites, *white arrow*) from Hg1 in the Rambla Honda-2 section. Note also the bioclastic infilling with ferruginous macro-oncoids and ammonoid fragments

(c) dense webs of straight filaments with common dichotomous branching, interpreted as green algae.

Taphonomy of macroinvertebrate fossil assemblages

The analysis of the fossil macroinvertebrates focused on the best-exposed surfaces with relatively abundant fossil remains, that is, on Hg1 (Lower–Middle Bathonian boundary), Hg2 (Middle–Upper Bathonian boundary), and Hg5 (Callovian–Oxfordian boundary). The macroinvertebrate assemblage is dominated by ammonoids in variable proportions (73–86% of the total fauna in Hg2, Fig. 10a; and 98% in Hg5, Fig. 10b). Other components are belemnites and scarce benthic organisms (gastropods and brachiopods).

The shelly fossils are preserved as neomorphic calcite regardless of the hardground. The limestone microfacies within the moulds and in the surrounding sediment occasionally differ. The ammonoid moulds are filament wackestones or *Globuligerina*-wackestones. In Hg2 and Hg5 of the Quípar section, the largest ammonoids (Figs. 10, 11a) have geopetal fills (red micrite and sparite) in the inner chambers of the phragmocone. Some of these ammonoids have chambers devoid of sediment but filled with calcite (Fig. 11a).

The mean ammonoid size is ~10 cm in Hg1 and Hg2 and ~7 cm in Hg5. The belemnites have a mean size of 15.1 cm. The fragmentation index (F_i, sensu Olóriz et al. 2002) is 33% in Hg1 and Hg2, and 44% in Hg5. Fragmentation mainly affected the living chamber and the most external whorls of the phragmocone (Fig. 10). Aptychi are scarce. The ammonoids lie preferentially parallel (>62%) to the hardground surfaces (Fig. 10), therefore originally in a sub-horizontal position. The belemnites and ammonoids are mainly orientated close to N–S in the Middle–Upper Bathonian hardground (Hg2) cropping out in the Quípar Unit. However, there are fluctuations in the plan-view orientation of the remains on the hardground depending on shell size (Reolid et al. 2010).

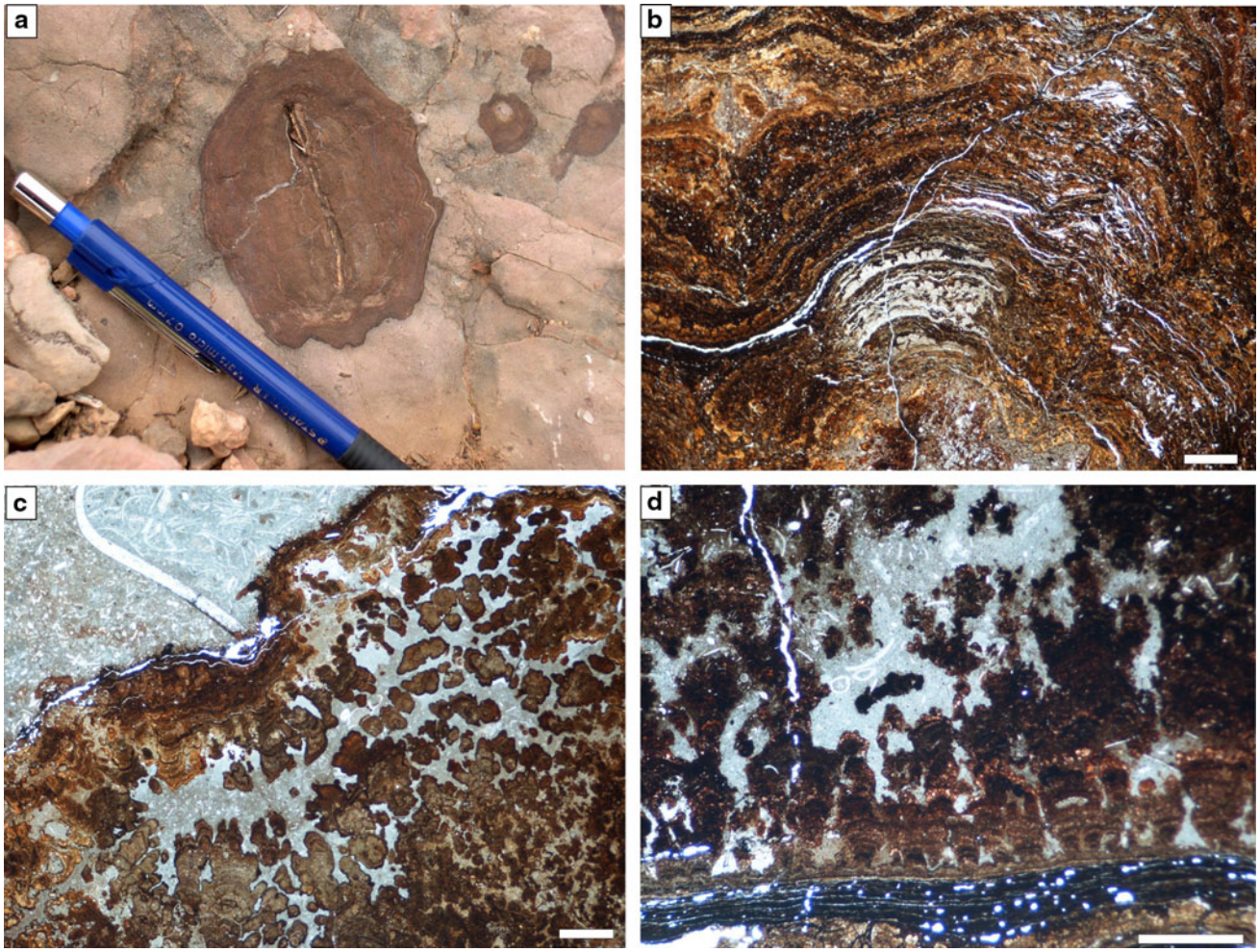

Fig. 9 **a** Field view of a ferruginous macro-oncoid from Hg5 in the Quípar section. **b** Ferruginous microbial laminated fabric from Hg5 in the Quípar section (*scale bar* 1 mm). **c** Arborescent microbial laminated fabric (*Frutexites*) from Hg5 in the Quípar section (*scale bar* 1 mm). **d** Arborescent laminated fabric (*Frutexites*) from Hg1 + 2 in the Lúgar 62-1 section (*scale bar* 1 mm)

Corrasion is common in Hg2 (Fig. 10a), affecting mainly the ammonoid living chamber and upper surface. Some ammonoids in this hardground in the Lúgar 62-1 and Quípar sections exhibit anchor facets. Other facets have been observed in specimens from Hg5 in the Quípar section with the growth of ferruginous coatings (Figs. 10b, 11b).

The encrustation index (E_i) ranges from 14.5% in Hg1 and Hg2 to 66.6% in Hg5. These encrustations are actually microbial ferruginous crusts, which occasionally built macro-oncoids.

Trace fossils

Hardgrounds and condensed facies from pelagic and hemipelagic environments constitute complex contexts for trace-fossil analysis due to the superposition of several ichnofacies. The best hardground exposures for ichnological analysis are those of the Lower–Middle Bathonian (Hg1) from the Reclot (Fig. 8b, c) and Cantón tectonic units, whereas in some parts of the Lúgar–Corque unit the trace fossils are related to the Middle–Upper Bathonian stratigraphic break (Hg2).

The most common trace fossil in Hg1 and Hg2 is *Thalassinoides*. The burrows are exceptionally well preserved and dense in the Rambla Honda-1 (Reclot Unit, Fig. 8b) and the Boquera sections (Cantón Unit). The gallery diameter of *Thalassinoides* is approximately 2.5 cm, but vertical galleries are not preserved. In the example from the Rambla Honda-1 section, the branched horizontal trace fossils have irregular walls forming positive epireliefs, 1 cm thick and 0.5–1 cm high with respect to the hardground surface (Fig. 8b). This epirelief could be related to an infaunal burrow network stabilized by a mucus-lined wall that experienced early diagenetic lithification. Subsequent erosion of the overlying, still soft sediment produced the epirelief.

In the Rambla Honda-1 section, other trace fossils co-exist with *Thalassinoides* in the Hg1 hardground (Fig. 8c). They comprise paired vertical tubes (perpendicular to the

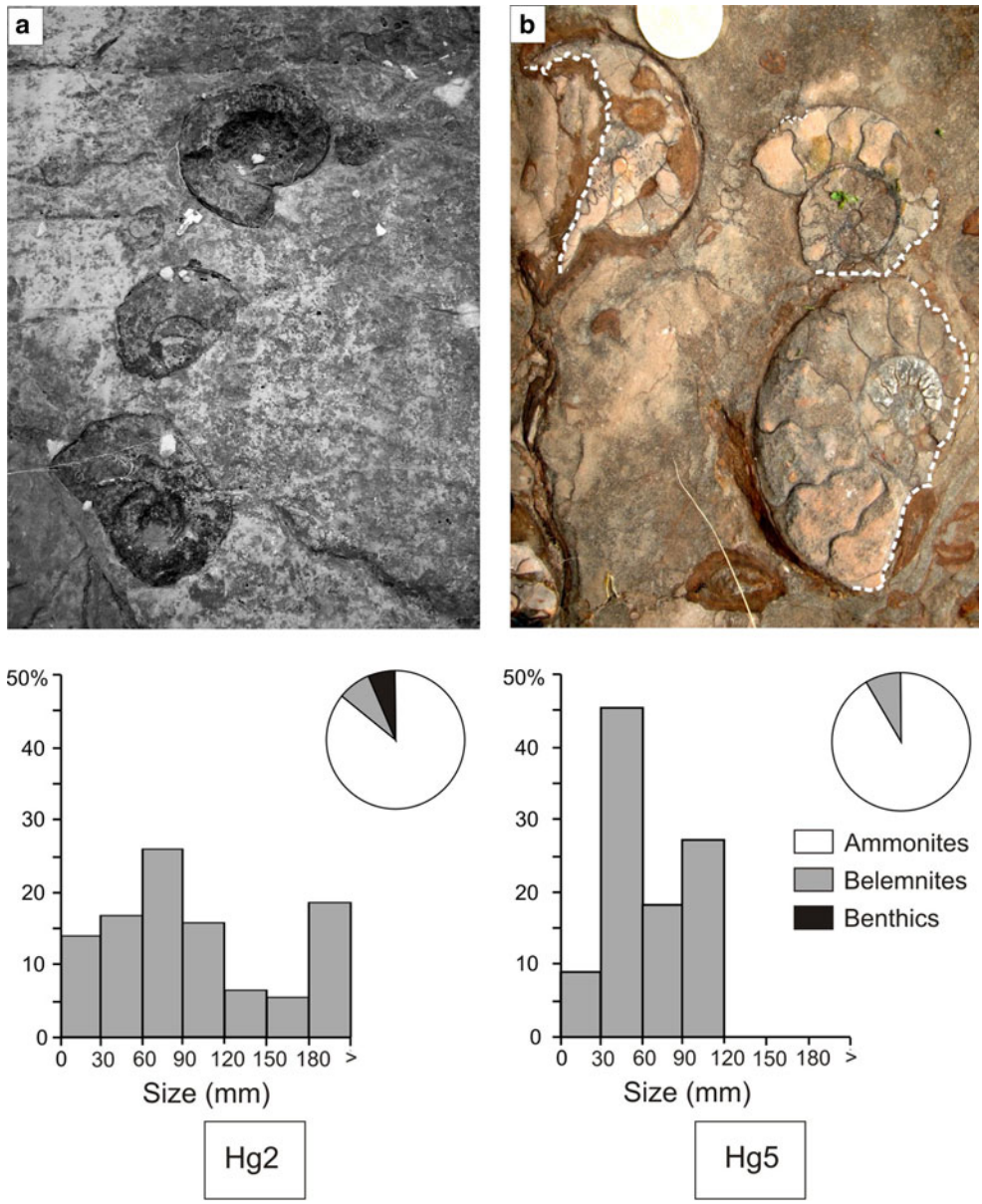

Fig. 10 Bedding plane view of ammonoids in Hg2 (**a**) and Hg5 (**b**), both from the Quípar unit. Also is shown the size distribution of the ammonid shells and the relative abundance of ammonoids, belemnites, and benthic organisms

hardground surface) with a circular cross-section (8–25 mm in diameter and 8–37 mm between tubes). These trace fossils have been assigned to *Arenicolites* by Reolid et al. (2010). Also on this surface, isolated vertical tubes with a circular cross-section (2 cm in diameter) are common; they bored into previous trace fossils and ammonoid moulds, and can be attributed to the *Trypanites* ichnofacies.

Neptunian dykes

Quípar unit

Neptunian dykes in this unit are related to the Hg2, Hg3, and Hg5 surfaces. Dykes related to Hg2 are characterized by straight walls with a maximum width of 10 cm. Sediment filling the dykes is a bio-packstone with filaments (*Bositra buchi*), *Globuligerina* sp., peloids, echinoderms, ammonoid moulds, and undifferentiated bioclasts. Two families of neptunian dykes have been observed. The main fracture family has a restored strike of N10°E–N30°E (Fig. 12) and is responsible for the stepped morphology of Hg2 in the Quípar section (Fig. 13a, b). The secondary fracture family has a restored strike of N110°–120°E (Fig. 12) and cuts the neptunian dykes of the main family, with a lateral displacement of nearly 7 cm.

The Lower–Middle Callovian hardground (Hg3) has narrow neptunian dykes (2 cm wide) with flat walls and a restored strike of N120°E. They have the same microfacies as the Hg2 neptunian dykes.

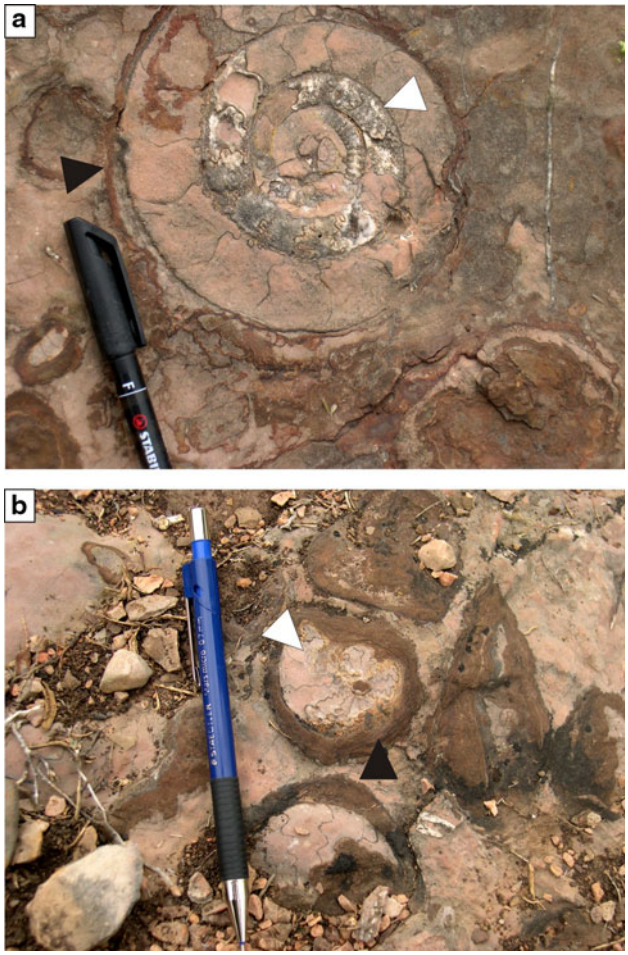

Fig. 11 Taphonomic features from ammonoids in Hg5 of the Quípar section. **a** Ammonoid with thin ferruginous crust (*black arrow*) and calcite cement in the innermost whorls of the phragmocone (*white arrow*). **b** Ammonoids with ferruginous coating forming a macro-oncoid produced by benthic microbial communities

Finally, hardground Hg5 is characterized by narrow neptunian dykes with two different orientations (N60°E and N140°E). The main difference between the neptunian dykes related to Hg5 and the other dykes is the presence of endostromatolites in the former.

Lúgar–Corque unit

Neptunian dykes in this unit are associated with Hg1 in the Lúgar 62-1 and Lúgar 62-2 sections (Figs. 12, 13c). Dyke walls are flat and the distance between walls ranges from <1 to 36 cm. The widest neptunian dykes are filled with

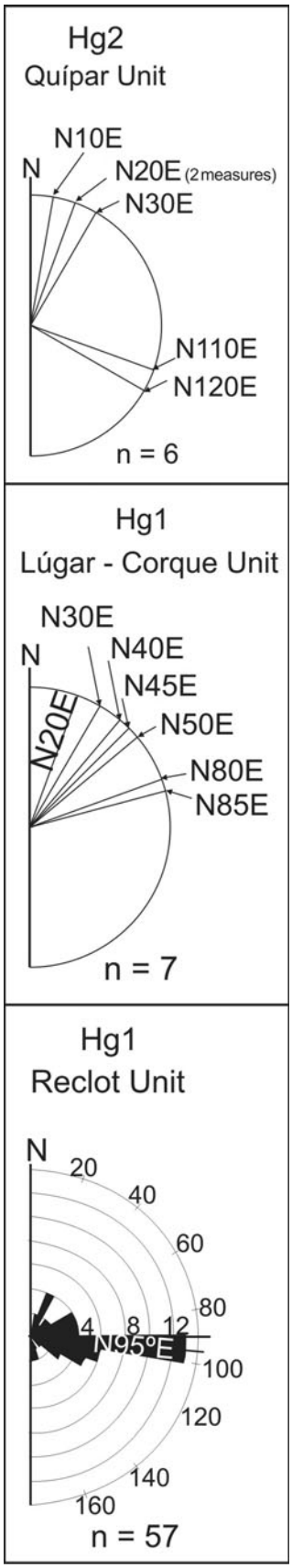

Fig. 12 Diagrams showing the line of strike of neptunian dykes related to certain stratigraphic breaks, after restoring stratification to the horizontal position (*n* number of strikes measured in the neptunian dykes) ▶

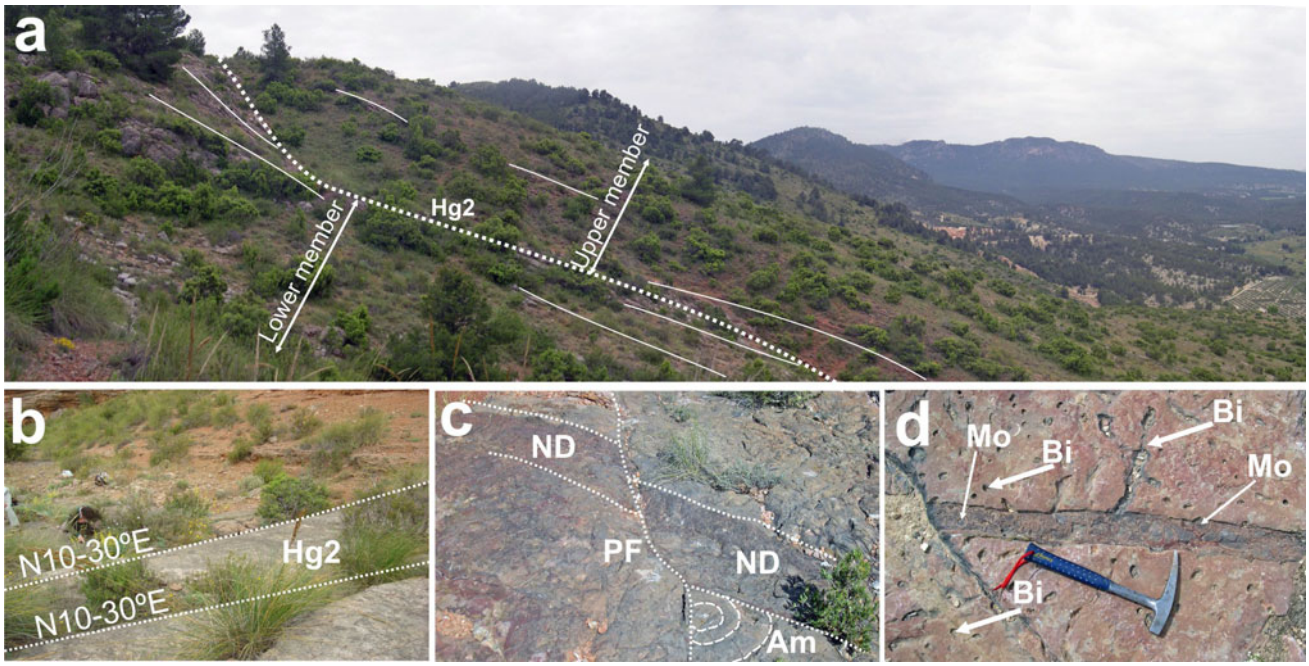

Fig. 13 **a** Panoramic view of the geometry of the Hg2 stratigraphic break in the Quípar unit. It shows the stepped morphology of this surface and the onlap of strata of the upper member. **b** Paleofractures of the Quípar section belonging to the N10-30°E system; these cut the Hg2 hardground. **c** Neptunian dyke (ND) in the Lugar 62-2 section (see Fig. 5). *Am* ammonite, *PF* paleofault. **d** Neptunian dyke (ND) in the Rambla Honda-2 section (see Fig. 5); *Bi* bioturbation, *Mo* macro-oncoids

filament- and *Globuligerina*-wackestone, including ferruginous macro-oncoids. Narrower neptunian dykes are made up of red micrite (mudstone). Dyke orientation ranges from N20°E to N50°E (Fig. 12). Some neptunian dykes are cross-cut by straight or slightly curved paleofaults with a N80–85°E restored strike; the lateral displacement is around 30 cm (Fig. 13c).

Cantón unit

Very small neptunian dykes are associated with the Hg1 hardground. They have straight or slightly irregular walls. Dykes with a width of 0.5–1 m consist of red micrite (filament and peloid-bearing wackestone-packstone). Wider dykes (10–40 cm) are filled with coarser-grained sediments, occasionally with a calcarenitic texture and with many small fossils (brachiopods, gastropods, bivalves, and belemnites), which more commonly are found in the deepest part of the neptunian dyke. Microfacies in such dykes are filament packstones in their lower part and *Globuligerina* wackestones in the upper part.

Reclot unit

The neptunian dykes are related to Hg1 (Fig. 8c). They constitute marine (pelagic, in this case) sediment fillings of long fissures within the underlying sediment. The fissures, from a few centimeters to decameters long, have smooth or slightly irregular walls varying in width from <0.5 to 37 cm. When the width is less than 4 cm, the neptunian dyke is filled with red micrite with iron oxyhydroxides. Wider neptunian dykes are characterized by a thin ferruginous laminated crust with locally arborescent morphologies (like *Frutexites*) growing from the walls inwards (Fig. 8d). These kinds of encrustations are called endostromatolites (Monty 1984; Martín-Algarra and Vera 1994; Martín-Algarra and Sánchez-Navas 1995, 2000; Burkhalter 1995). They can also be partially filled with coarser-grained sediments including ferruginous macro-oncoids (Fig. 8d) or fragments of Fe–Mn-rich crusts. The microfacies is a packstone with bioclasts (brachiopods, echinoderms, and bivalves), filaments (*Bositra buchi*), *Globuligerina*, benthic foraminifera (e.g., *Protopeneroplis striata*, *Valvulina lugeoni*), radiolaria, and peloids. These microfacies are similar to the Callovian bioclastic bed (facies 2, Table 1). The main strike of neptunian dykes, after restoring stratification to the horizontal position, ranges from N90°–100°E (Fig. 12). These originally subvertical neptunian dykes cut ammonoid moulds and trace fossils (Fig. 13d).

Discussion

This section is divided into two parts. The first one is an analysis of the data related to neptunian dykes; its purpose is to discuss the possible controls of Jurassic synsedimentary

tectonics on sedimentation in this part of the South Iberian Paleomargin. The second part discusses the evolution of the sedimentary environments considering the information derived from all analyzed features (microfacies, ferruginous crusts, taphonomy of macroinvertebrates, and trace fossils) related to discontinuities and described above.

Synsedimentary tectonics

Neptunian dykes are indicative of synsedimentary tectonics, probably related to tensional deformation systems (e.g., Molina et al. 1995; Martire and Pavia 2004; Crne et al. 2007; Basilone 2009; Bertok and Martire 2009). According to Ziegler (1989), the Middle–Late Jurassic transition was a tectonically active period with a change from extensional to transtensional conditions in the Western Tethys. This has been recorded in Western Sicily (Martire and Pavia 2004; Basilone 2009; Bertok and Martire 2009), the Iberian Cordillera (Salas et al. 2001), the Betic Internal and External zones (Vera et al. 2004), and the Internal Rif (Kadiri 2002).

In the Eastern External Subbetic, most neptunian dykes (Fig. 12) are related with the stratigraphic break Hg1 (top of the Lower Bathonian) and Hg2 (top of the Middle Bathonian). These breaks are interpreted to be related to two main deformation phases. Moreover, in the Quípar Unit, other neptunian dykes have been recorded related to the Hg3 (Lower–Middle Callovian boundary) and Hg5 (Callovian–Oxfordian boundary) hardgrounds (Fig. 7), but the number of neptunian dykes studied in relation to them is very low.

According to Vera (2001), the change from an extensional to a transtensional tectonic regime occurred during the Callovian–Oxfordian boundary at the South Iberian Paleomargin. Nevertheless, the presence of neptunian dykes associated with Hg1 and Hg2 (and therefore prior to this time) indicates the existence of earlier tectonic histories.

In Hg1, three main systems of neptunian dykes have been identified (Fig. 12), with restored strikes of N20°–50°E (mean value N35°E), and N80°–85°E (mean value N82.5°E), both in the Lúgar–Corque Unit, and N90°–100°E (Reclot Unit), with a mean value of N95°E. Based on paleomagnetic data from the Eastern External Subbetic, Platzman and Lowrie (1992) estimated that the mean clockwise vertical axis rotation for the Subbetic was 60°. If the value of the mean clockwise rotation of the Subbetic is subtracted from the present restored strike of the neptunian dykes from the Lúgar–Corque and Reclot units, the resulting strike for these structures would be N140°–170°E (mean value N155°E) and N20°–25°E (mean value N22.5°E) (Lúgar–Corque Unit), and N30°–40°E (mean value N35°E, Reclot Unit). Whether or not one takes into account the rotation calculated by Platzman and Lowrie (1992), it is clear that the fracture system affecting the pelagic swell represented by the Lúgar–Corque Unit was different from that determining the evolution of the pelagic swell represented by the Reclot Unit (Nieto 1997).

In the Lúgar–Corque Unit, two different systems are found; the older system of fractures is made up of neptunian dykes with a mean restored strike of N35°E, and is crossed by another system of fractures with a mean strike of N82.5°E. The angle between the two neptunian dyke systems is 47.5°. According to Hancock (1985, 1994), two fracture systems forming a dihedral angle ranging between 10° and 50° are hybrid fractures with a mixed tensional and shear deformation. Therefore, the pelagic swell represented by the Lúgar–Corque Unit records neptunian dykes generated by transtensional tectonics. In the Reclot Unit, there is one main system of neptunian dykes, with a nearly E-W restored mean orientation related to Hg1, therefore resulting from an extensional stage that affected this pelagic swell in late Bathonian time.

In relation to Hg2, in the Quípar Unit, two systems of neptunian dykes have been documented (Fig. 12), with restored strikes of N10°–30°E (mean value N20°E) and N110°–120°E (mean value N115°E). Taking into account the paleomagnetic rotation calculated by Platt et al. (2003) for this tectonic unit (54° in the clockwise sense), their preorogenic orientation should be N136°–156°E (mean value N146°E) and N56°–66°E (mean value N61°E), respectively. The first system controlled the stepped geometry of the Hg2 surface (Fig. 13a, b), and it was possibly the consequence of an initial tensional phase that affected the pelagic swell. The N110°–120°E fractures cut the previous ones. As the dihedral angle between the two restored strikes is 95°, this second system of neptunian dykes could have developed in a sinistral wrenching setting (Hancock 1985, 1994), according to the regional deformation regime that affected the South Iberian Paleomargin in the Middle–Late Jurassic transition. The sinistral wrenching deformation was probably active in the Early–Middle Callovian time.

The shear deformation stage of the margin probably persisted up to the Callovian–Oxfordian boundary (Hg5) as can be deduced from the presence of neptunian dykes with restored strikes between N60°E and N140°E and a dihedral angle of 80°, which according to Hancock (1985, 1994), is typical of fractures developing under shear stress.

Nieto and Rey (2004) have shown that a fault system with a present-day average strike close to E-W and parallel to the present-day Crevillente Fault Zone (CFZ) controlled the stratigraphic features of the Eastern External Subbetic pelagic swells. This fault system could be interpreted in relation to Middle–Late Jurassic extensional–sinistral tectonics that affected the South Iberian Paleomargin, which was possibly related to the seafloor spreading of the Tethys and central Atlantic oceans. This geodynamic context could

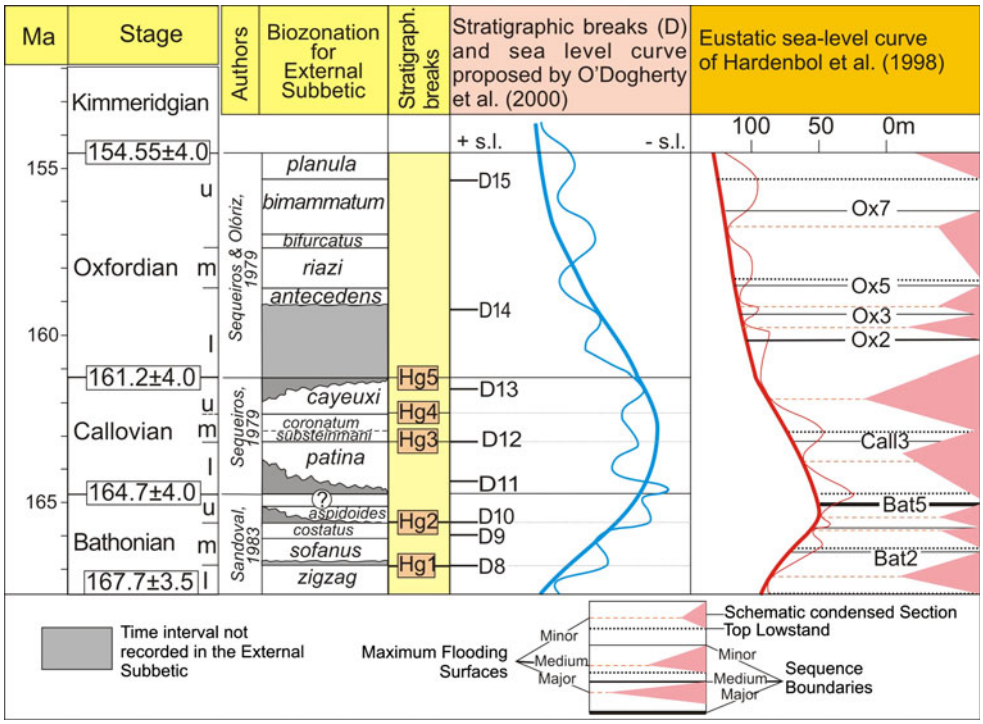

Fig. 14 Correlation between the stratigraphic breaks studied in this paper, the discontinuities shown by O'Dogherty et al. (2000), the sea-level curve proposed by these authors, and the eustatic sea-level curve proposed by Hardenbol et al. (1998)

have been responsible for the origin of synsedimentary open fractures that were later filled with pelagic sediments to constitute neptunian dykes.

Evolution of the sedimentary environments

Some authors propose an eustatic sea-level fall during the Bathonian (e.g., Hardenbol et al. 1998). Vera (1988), Vera and Martín-Algarra (1994) and O'Dogherty et al. (2000) also reported a sea-level fall for the South Iberian Paleomargin (Fig. 14). Several authors, (e.g., Vera 2001; Vera et al. 2004) showed that at this continental margin of the Western Tethys rifting developed in a transtensional tectonic regime during the Middle–Late Jurassic transition. Moreover, Vera and Martín-Algarra (1994), and later Martín-Algarra and Sánchez-Navas (2000), reported that the origin of sedimentary breaks and associated condensation surfaces such as P–Fe–Mn-rich microbial structures formed during the Middle–Upper Jurassic transition (some recognized in the same areas studied in this paper), were related to a complex interplay between synsedimentary tectonics, submarine hydrothermal activity, and sea-level changes. In short, the Jurassic pelagic swells, where the studied External Subbetic condensed pelagic successions were deposited, developed in relation to this geodynamic framework (Fig. 15a). In this pelagic context, signals of the changes in sea level and tectonic-rifting processes interfered, and are recorded as stratigraphic breaks. The problem is how to differentiate between the two kinds of signals, and how to attribute the observed features to the two different types of processes, respectively related to sea-level changes and to tectonics.

In previous papers, several authors interpreted the record of the stratigraphic discontinuities separating platform and pelagic carbonate facies as the result of tectonics (e.g., Clari et al. 1995; Crne et al. 2007; Olóriz et al. 2008; Basilone 2009; Bertok and Martire 2009). These authors showed that the superposition of pelagic sediments on carbonate platforms records the drowning -or collapse- of the platform below the depth of the maximum carbonate production (euphotic zone). First, the tectonic collapse occurred, and then the development of the unconformity. The situation analyzed in the present research is different, because the rocks under- and overlying the unconformity surfaces studied here (hardgrounds) were generated in pelagic environments and, consequently, there are no sharp facies changes between them. In this context, reconstructing the chronological order of features attributed to sea-level changes and those to tectonic mechanisms is more complex. In the paragraphs below, each of the discontinuities considered here is analyzed and a chronological order of the features associated with them is proposed.

Hg1: Lower–Middle Bathonian boundary

The hiatus related to Hg1 lasted between 2 to 9.2 Ma (geochronometry according to Ogg 2004; see Fig. 7), depending on the tectonic unit considered and the outcrop. This unconformity can be correlated with the D8 of O'Dogherty et al. (2000), who interpreted it as a consequence

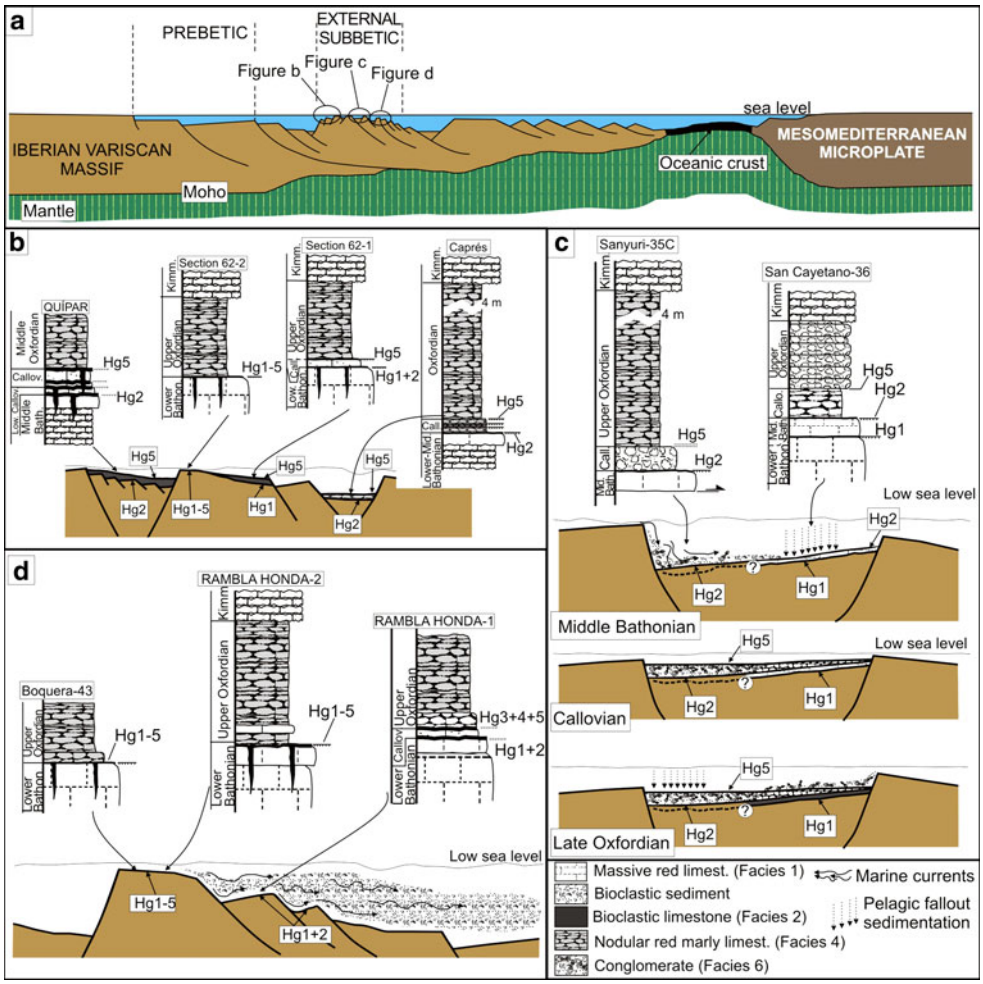

Fig. 15 **a** Model of the South Iberian Paleomargin for the Middle Jurassic–Early Cretaceous after Vera (2001). **b–d** Tectonosedimentary setting of the stratigraphic sections with the main discontinuities (Hg1, Hg2, and Hg5) from the Quípar, Lúgar–Corque, Crevillente, Cantón and Reclot units. For legend of the stratigraphic sections, see Fig. 5

of sea-level fall (Fig. 14). In the Hg1, trace fossils and taphonomic features indicate a halt in sedimentation and incipient lithification of the sea bottom with a change from softground to hardground. *Arenicolites* and *Thalassinoides* from the softground stage and borings from the hardground stage are identified in the Reclot Unit (Fig. 8b, c). *Thalassinoides* is the dwelling burrow of decapod crustaceans (e.g., Bromley and Frey 1974; Svarda and Bottjer 1988; García-Ramos et al. 1989), usually interpreted as a component of the *Cruziana* ichnofacies, which is characterized by moderate energy conditions and soft substrates (Ekdale et al. 1984; Pemberton et al. 1992; McEachern et al. 2007). *Arenicolites* has been related to infaunal suspension-feeder organisms living in high-energy shallow-marine environments, and being a component of the *Skolithos* (Pemberton et al. 1992) and *Cruziana* ichnofacies (McEachern et al. 2007), which implies softground conditions. The borings cutting through previous trace fossils and ammonoid moulds are indicative of a hard substrate. The superposition of ichnofabrics reflects successive stages of substrate lithification (e.g., Bromley 1975; Bromley and Ekdale 1986; Fürsich et al. 1992).

In some outcrops, the ammonoid moulds show signs of corrasion and anchor facets. The intensity of the corrasion processes was related to the residence time of the remains on the sea bottom, allowing erosion by bottom currents, bioerosion, and/or submarine dissolution. A reduced sedimentation rate and sediment bypassing favored the exhumation, faceting, and reworking of the moulds.

According to Clari et al. (1995) and Rais et al. (2007), a low sea level is coupled with climate changes and an increase in the magnitude of marine currents, thereby hampering sediment accumulation and favoring erosion. Simultaneously, the seafloor becomes progressively cemented, thereby forming a hardground. The discontinuity recorded by Hg1 is potentially correlated with the global cooling episode during the Middle Bathonian proposed by Dromart et al. (2003b) and Rais et al. (2007).

The neptunian dykes associated with Hg1 (Figs. 8c, 12, 13d) are related to fractures that developed in a transtensional tectonic setting (Fig. 15; e.g., Nieto 1997; Bertok and Martire 2009), as analyzed in the previous chapter. This tectonic activity was subsequent to the hardground development, as the neptunian dykes intersect the trace

fossils and the ammonoid moulds (Fig. 13d). The fractures were filled with bioclastic sediment with ferruginous macro-oncoids and ferruginous endostromatolites on the walls (Fig. 8d). The identification of *Frutexites* in these fractures is congruent with the cryptic habitat inferred for this type of micro-organisms (Reolid and Molina 2010).

In some outcrops (Quípar, Lúgar 62-1, San Cayetano-36 and Rambla Honda-1 sections), a bioclastic bed (facies 2, Table 1, Figs. 3f, 4b) with ferruginous macro-oncoids is recorded above Hg1. Based on the coexistence of chemosynthetic and photosynthetic micro-organisms in the ferruginous macro-oncoids, Reolid and Nieto (2010) inferred a bathymetry of 50–100 m for the sea bottom. The current induced bypassing of bioclastic sediment and reworking of previous material. These currents incorporated the ferruginous macro-oncoids from the hardground surface into the bioclastic bed and also in the sedimentary fill of the fractures, resulting in later neptunian dykes (Fig. 15d).

On the same pelagic swell, the morphology of the bottom can be irregular or stepped (Fig. 15) because of the different fracture systems. Some pelagic swells, in which the bioclastic bed disappears laterally (as in the Lúgar–Corque or Reclot units), may have had a tilted topography produced by listric faults activity (Fig. 13b, d) (Molina et al. 1999). In the sheltered depressions, sediment accumulated forming the bioclastic beds. In contrast, topographic highs on pelagic swells were current-swept, sediment was by-passed, and erosion and/or non-deposition persisted from the Middle Bathonian to the Late Oxfordian (Lúgar 62-2 and Boquera 43 sections, Figs. 7, 15b, d).

Hg2: Middle–Upper Bathonian boundary

This hardground is equivalent to D10 of O'Dogherty et al. (2000) (Fig. 14). These authors relate this stratigraphic break to a fall in sea level, but it does not coincide with the major sequence boundary Bat5 proposed by Hardenbol et al. (1998), which would result from a very important eustatic lowstand (Fig. 14). The trace fossils and taphonomic features of Hg2 are very similar to those described in Hg1. It is characterized by ferruginous crusts and the presence of neptunian dykes. The beginning of sedimentation after Hg2 is also recorded by a conglomerate level with reworked Callovian ammonites (Sanyuri 35C, Crevillente Unit; Fig. 15c) or by a bioclastic bed (Quípar and Lúgar–Corque units; Fig. 15b). As for Hg1, we interpret the hiatus as a consequence of relative sea-level fall followed by transtensional tectonics and renewed sedimentation due to tectonics or to the effect of marine currents.

The time interval between Hg1 and Hg2 includes the *Sofanus* and *Costatus* biozones (approximately 1.5 Ma, according to Ogg 2004; Figs. 7, 14). In some sections, sedimentation of the Ammonitico Rosso facies continued during the Middle Bathonian because in the pelagic swells the presence of sheltered areas or topographically low settings developed and favored the sediment accumulation and preservation (Quípar and Crevillente units, and part of the Lúgar–Corque Unit; Figs. 7, 15b, c, d).

The taphonomic features of Hg2 indicate its evolution from a softground to hardground. Large ammonoids with the innermost chambers of the phragmocone unfilled or partially filled with sparite indicate fast burial, which complicates the chamber infilling by sediment usually favored by long-lasting exposure with corrasion, fragmentation, and boring. Initially, the sediment was soft, as suggested by the vertical orientation of some large ammonoids.

The subsequent halt in sedimentation related to Hg2 development progressively hardened the sediment and preserved ammonoid shells as neomorphic calcite, due to early diagenesis (submarine cementation and/or recrystallization of the originally aragonitic shell) typical of hardgrounds. Sediment hardening was probably coeval with partial filling of the ammonoid shells by sparitic cements (Reolid et al. 2010). As a result of the lack or low rate of sedimentation, the ammonoid remains were commonly exhumed, facetted, and reworked (Fig. 10a). Reolid et al. (2010) propose that the smallest ammonoids were orientated by weak currents, probably fair-weather currents, whereas larger ammonoids were rearranged by stronger currents.

When it is biostratigraphically detected, the stratigraphic gap associated with Hg2, lasted approximately 0.5 Ma (Fig. 7) before sedimentation of the condensed Callovian bioclastic bed. As this bed includes ferruginous macro-oncoids and reworked Middle Bathonian ammonoids, it becomes evident that, during its deposition, conditions were favorable for the growth of chemo-organotrophic benthic microbial communities (Reolid and Nieto 2010), which precipitated Fe–Mn oxyhydroxides coating the ammonoids and resulting in macro-oncoids or any other available type of firm or hard substratum (see also Martín-Algarra and Sánchez-Navas 1995). The development of benthic microbial communities was possible due to the low sedimentation rate and, perhaps also, to the input of large amounts of Fe, Mn, some trace elements, and REE, probably associated with contemporaneous submarine hydrothermal and volcanic activity in neighboring areas of the Middle Subbetic basin (Vera and Martín-Algarra 1994; Vera et al. 1997).

On the pelagic swell represented by the Crevillente Unit (Fig. 15c), sedimentary instability would have been important with the development of conglomerates (facies 6, Table 1; Fig. 3c) containing fragments of Callovian ammonoid moulds.

Hg3 (Lower–Middle Callovian boundary) and Hg4 (Middle–Upper Callovian boundary)

Both the Callovian bioclastic bed and the conglomerates directly on Hg2 may be interpreted as a result of high-energy conditions described in other hardground examples during the onset of transgression (e.g., Martire 1992; Olóriz et al. 2008). According to Clari et al. (1995), locally intense marine currents may be related to paleogeographic re-organization. This agrees with the final configuration of the Hispanic Corridor during the Callovian and the ensuing re-organization of the paleogeography and paleoceanography from the Pacific Ocean to the Western Tethyan regions through the newborn (and still narrow) Central Atlantic Ocean, which allowed the start of circumequatorial oceanic circulation (Rais et al. 2007). The origin of hardgrounds at the Lower–Middle Callovian boundary (Hg3) and the Middle–Upper Callovian boundary (Hg4) can be tentatively correlated to this event. These discontinuities are recorded only in the westernmost part of the study area (Quípar and Lúgar–Corque units). These hardgrounds are associated with condensed bioclastic beds with ferruginous macro-oncoids and reworked ammonoids.

Hg3 coincides with a minor sea-level fall (Fig. 14) and is correlated with D12 of O'Dogherty et al. (2000), which they consider to be a consequence of a fall in sea level. However, the presence of neptunian dykes in some outcrops of this discontinuity could explain their development as a consequence of tectonic processes. In neighboring domains of the South Iberian Paleomargin, such as the Iberian Chain, Ramajo and Aurell (2008) interpreted the condensed facies at the end of the Callovian as the result of a eustatic sea-level fall. Hg4 coincides with the beginning of another minor-order sea-level fall, but we have not been able to correlate it with any discontinuity of O'Dogherty et al. (2000) and Hardenbol et al. (1998) (Fig. 14), which suggests it is purely local.

Hg5 (Callovian–Oxfordian boundary)

This discontinuity could be correlated to D13 of O'Dogherty et al. (2000) (Fig. 14), who interpreted it as related to the beginning of a sea-level fall. However, scarce biostratigraphic data make a precise correlation difficult. The associated bioclastic beds and fragmented and reworked ammonoids indicate significant marine currents over the pelagic swells (Fig. 15b, c, d). The sea-level fall stopped sedimentation and favored early diagenesis leading to hardground development, as well as to corrasion of ammonoid remains (Fig. 11).

Neptunian dykes in the Quípar Unit are related to a new local tectonic episode. Both the sea bottom and fracture walls were colonized by ferruginous microbial crusts with features similar to those described in previous hardground surfaces.

During the Callovian–Oxfordian boundary, transtensional tectonics in the South Iberian Paleomargin were related to the complete break-up of the African Plate, the Iberian Plate, and the Mesomediterranean Microplate, with the opening of narrow oceanic basins in between (Vera 2001). Azeredo et al. (2002) analyzed this event in the Lusitanian Basin and interpreted it in relation to changes in the position of the Mid-Atlantic Ridge. Combined with the ongoing opening of the Atlantic and Tethys oceans (Gradstein et al. 1991; Stampfli and Borel 2002), the Middle Oxfordian sea-level rise (Haq et al. 1988; Hallam 2001) favored the reorganization of ocean currents in the Atlantic-Tethys system (Pellenard et al. 1999; Bombardiere and Gorin 2000; Bill et al. 2001; Leinfelder et al. 2002; Louis-Schmid et al. 2007).

The beginning of the Oxfordian sedimentation was diachronous, and probably controlled by local configuration of each part of the Eastern External Subbetic pelagic swell area (Fig. 15). In the Caprés section of the Lúgar–Corque unit, the upper member of the UAR Formation includes the Lower Oxfordian (Checa and Sequeiros 1990). This small depocenter probably developed as a consequence of the existence of shelter areas on top of pelagic swells or topographically low settings. In both the accumulation and preservation of sediment were important (Fig. 13b). In the Quípar unit, the base of the upper part of the UAR Formation is Middle Oxfordian, probably related to a sheltered sedimentary setting (Fig. 15b). In the other sections, sedimentation began in the late Oxfordian because of their position on non-subsiding pelagic swells, where due to currents sediment bypassing was significant. Sedimentation conditions in the Crevillente Unit were more unstable allowing the deposition of conglomerates (Fig. 15c).

The onset of the Oxfordian sedimentation in the External Zones of the Betic Cordillera and also in other domains of the Western Tethys was favored by a major reorganization of global oceanic currents due to the definitive opening of the Atlantic and Tethys oceans combined with sea-level rise, which allowed the formation of a circumglobal seaway (Pellenard et al. 1999; Bill et al. 2001; Louis-Schmid et al. 2007). Widespread and increasing carbonate accumulation at that time was due to the warmer and more arid climate during the Late Oxfordian-Kimmeridgian (Podhala et al. 1998; Price and Gröcke 2002; Dromart et al. 2003a, b; Lécuyer et al. 2003; Price and Rogov 2009), the availability of new habitats for marine communities due to the sea-level rise (Leinfelder et al. 2002; Cecca et al. 2005), and changing ocean currents (Abbink et al. 2001; Rais et al. 2005) favoring nutrient re-distribution.

Conclusions

The integrated analysis of the studied microfacies, ferruginous crusts (geochemical and mineralogical), taphonomy, ichnology, and neptunian dykes, placed in a biostratigraphic context, lead us to the following conclusions:

1. The Middle Bathonian to Middle Oxfordian interval in the Eastern External Subbetic is characterized by the presence of five stratigraphic discontinuities represented by hardgrounds: Hg1 (Lower–Middle Bathonian boundary), Hg2 (Middle–Upper Bathonian boundary), Hg3 (Lower–Middle Callovian boundary), Hg4 (Middle–Upper Callovian boundary), and Hg5 (Callovian–Oxfordian boundary). The main regional unconformities are Hg1, Hg2, and Hg5, which are found in most tectonic units, whereas Hg3 and Hg4 are merely local.
2. Abundant fossil macroinvertebrates with taphonomic traits evidencing corrasion, early diagenetic processes, and reworking are associated with Hg1, Hg2, and Hg5. Some of these surfaces contain trace fossils of the *Cruziana* and *Trypanites* ichnofacies, which trace their evolution from softgrounds to hardgrounds.
3. Different families of neptunian dykes are recorded in relation to these hardgrounds. They cross-cut trace fossils and ammonoid moulds and indicate tectonic activity in the studied epi-oceanic paleoenvironments during the Bathonian–Oxfordian time interval. Tectonic conditions were extensional during the Bathonian and transtensional during the latest Callovian, according to the general geodynamic evolution of the segment of the South Iberian Paleomargin studied in this paper.
4. Hardground surfaces and fracture walls were colonized by ferruginous microbial crusts. Ferruginous macrooncoids are common within condensed bioclastic beds bounded by hardgrounds. These microbialites indicate low sedimentation rates and the potential influence of submarine volcanism in the neighboring Middle Subbetic, which led to enrichment in Fe, Mn, trace elements, and REE.
5. The hardgrounds development is interpreted in the light of sea-level falls leading to breaks in sedimentation, sediment bypassing, erosion, and early diagenesis. After halts in sedimentation, tectonic episodes are recorded as neptunian dykes. Fe-rich microbial accretions just above the hardground surfaces and on the walls of neptunian dykes, prior to deposition of the condensed bioclastic beds, may be interpreted as the first signs of the onset of transgression.
6. Different durations for each hiatus, the diachrony of the top of the lower member and of the base of the upper member of the UAR Formation, and lateral facies changes can be related to differences in water depth, probably due to stepped topography and tilting favored by listric faults bounding the pelagic swells. This resulted in differential subsidence between sections and/or tectonic units located in different parts of the basin and the development of sheltered areas at the top of pelagic swells where the sediment could be preserved.

Acknowledgments This research was carried out with the financial support of the research projects UJA_07_16_23 (Universidad de Jaén), CGL2008-03007, CGL2009-10329 (both of the Ministerio de Ciencia e Innovación), P08-RNM-03715 (Junta de Andalucía), RYC-2009-04316, and the Research Team RNM-200 Junta de Andalucía. We would like to thank Professors Franz Fürsich and Agustín Martín-Algarra for their interesting comments and remarks that improved the original manuscript. We are also indebted to Christine Laurin for the English version of the text. We are also grateful to Antonio Piedra, technician at the Laboratorio de Geología of the Universidad de Jaén, for preparation of the thin-sections.

References

Abbink O, Targarona J, Brinkhuis H, Visscher H (2001) Late Jurassic to earliest Cretaceous paleoclimatic evolution of the southern North Sea. Global Planet Change 30:231–256

Aurell M, Fernández-López S, Meléndez G (1994) The Middle–Upper Jurassic oolitic ironstone level in the Iberian Range (Spain). Eustatic implications. Geobios Mem Spec 17:549–561

Aurell M, Bádenas B, Bello J, Delvene G, Meléndez G, Pérez-Urresti I, Ramajo J (1999) El Calloviense y el Jurásico Superior en la Cordillera Ibérica Nororiental y la zona de enlace con la Cordillera Costero Catalana, en los sectores de Sierra de Arcos, Calanda y Xerta-Paüls. Cuad Geol Ibérica 25:73–110

Azeredo AC, Wright VP, Ramalho MM (2002) The Middle–Late Jurassic forced regression and disconformity in central Portugal: eustatic, tectonic and climatic effects on a carbonate ramp system. Sedimentology 49:1339–1370

Basilone L (2009) Mesozoic tectono-sedimentary evolution of Rocca Busambra in western Sicily. Facies 55:115–135

Bertok C, Martire L (2009) Sedimentation, fracturing and sliding on a pelagic plateau margin: the Middle Jurassic to Lower Cretaceous succession of Rocca Busambra (Western Sicily, Italy). Sedimentology 56:1016–1040

Bill M, O'Dogherty L, Guex J, Baumgartner PO, Masson H (2001) Radiolarite ages in Alpine-Mediterranean ophiolites: constraints on the oceanic spreading and the Tethys-Atlantic connection. Geol Soc Am Bull 113:129–143

Bombardiere L, Gorin GE (2000) Stratigraphical and lateral distribution of sedimentary organic matter in Upper Jurassic carbonates of SE France. Sediment Geol 132:177–203

Brett CE, Baird GC (1986) Comparative taphonomy: a key to pale environmental interpretation based on fossil preservation. Palaios 1:207–227

Bromley RG (1975) Trace fossils at omission surface. In: Frey RW (ed) The study of trace fossils. Springer, Berlin Heidelberg New York, pp 399–428

Bromley RG, Ekdale AA (1986) Composite ichnofabric and tiering of burrows. Geol Mag 123:59–65

Bromley RG, Frey RW (1974) Redescription of the trace fossil *Gyrolithes* and taxonomic evaluation of *Thalassinoides*, *Ophiomorpha* and *Spongeliomorpha*. Bull Geol Soc Denmark 23:311–335

Burkhalter RM (1995) Ooidal ironstones and ferruginous microbialites: origin and relation to sequence stratigraphy (Aalenian and Bajocian, Swiss Jura Mountains). Sedimentology 42:57–74

Caracuel JE (1996) Asociaciones de megainvertebrados, evolución sedimentaria e interpretaciones ecoestratigráficas en umbrales epioceánicos del Tethys Occidental (Jurásico superior). PhD Thesis, Universidad Granada, p 458

Cecca F, Martin-Garin B, Marchand D, Lathulière B, Bartolini A (2005) Palaeoclimatic control of biogeographic and sedimentary events in Tethyan and peri-Tethyan areas during the Oxfordian (Late Jurassic). Palaeogeogr Palaeoclimatol Palaeoecol 222:10–32

Checa A, Sequeiros L (1990) New data on the Lower Oxfordian from the Subbetic Zone (Betic Range, SE Spain). 1st Oxfordian Meeting, Zaragoza 1988. Publ Sepaz 1990:153–160

Clari PA, Dela Pierre F, Martire L (1995) Discontinuities in carbonate successions: identification, interpretation and classification of some Italian examples. Sediment Geol 100:97–121

Collin PY, Loreau JP, Courville P (2005) Depositional environments and iron ooids formation in condensed sections (Callovian–Oxfordian, south-eastern Paris basin, France). Sedimentology 52:969–985

Courville P, Collin PY (1997) La série du Callovien et de l'Oxfordien de Veuxhaulles (Châtillonnais, Côte d'Or): problèmes de datation, de géométrie et de paléoenvironnements dans une série "condensée". Bull Sci Bourgogne 49:29–43

Crne AE, Šmuc A, Skaberne D (2007) Jurassic neptunian dikes at Mt Mangart (Julian Alps, NW Slovenia). Facies 53:249–265

Dromart G (1989) Deposition of Upper Jurassic fine-grained limestones in the western Subalpine Basin, France. Palaeogeogr Palaeoclimatol Palaeoecol 69:23–43

Dromart G, Garcia J-P, Gaumet F, Picard S, Rousseau M, Atrops F, Lécuyer C, Shepard SMF (2003a) Perturbation of the carbon cycle at the Middle/Late Jurassic transition: geological and geochemical evidence. Amer J Sci 303:667–707

Dromart G, Garcia J-P, Picard S, Atrops F, Lécuyer C, Shepard SMF (2003b) Ice age at the Middle—Late Jurassic transition? Earth Planet Sci Lett 213:205–220

Ekdale AA, Bromley RG, Pemberton SG (1984) Ichnology. Trace fossils in sedimentology and stratigraphy. SEPM Short Course 15:1–316

Fürsich FT, Oschmann W, Singh IB, Jaitly AK (1992) Hardgrounds, reworked concretion levels and condensed horizons in the Jurassic of western India: their significance for basin analysis. J Geol Soc Lond 149:313–331

Fürsich FT, Singh IB, Joachimski M, Krumm S, Schlirf M, Schlirf S (2005) Palaeoclimate reconstructions of the Middle Jurassic of Kachchh (western India): an integrated approach based on palaeoecological, oxygen isotopic, and clay mineralogical data. Palaeogeogr Palaeoclimatol Palaeoecol 271:289–309

García-Hernández M, López-Garrido AC, Rivas P, Sanz de Galdeano C, Vera JA (1980) Mesozoic paleogeographic evolution of the external zones of the Betic Cordillera. Geol Mijnb 59:155–168

García-Hernández M, López-Garrido AC, Martín-Algarra A, Molina JM, Ruiz-Ortiz PA, Vera JA (1989) Las discontinuidades mayores del Jurásico de las Zonas Externas de las Cordilleras Béticas: análisis e interpretación de los ciclos sedimentarios. Cuad Geol Ibérica 13:35–52

García-Ramos JC, Valenzuela M, Suárez de Centi C (1989) Sedimentología de las huellas de actividad orgánica. In: Sedimentología. Nuevas Tendencias. CSIC 2:261–342

Gradstein FM, Gibbling MR, Sarti M, Von Rad U, Thurow JW, Ogg JG, Jansa LF, Kaminski MA, Westermann GEG (1991) Mesozoic Tethyan strata of Thakkola, Nepal, evidence for the drift and breakup of Gondwana. Palaeogeogr Palaeoclimatol Palaeoecol 88:193–218

Gygi RA (1981) Oolitic iron formations: marine or not marine? Eclogae Geol Helv 74:233–254

Gygi RA, Persoz F (1987) The epicontinental sea of Swabia (southern Germany) in the Late Jurassic: factors controlling sedimentation. N Jb Geol Paläont Abh 176:49–65

Hallam A (2001) A review of the broad pattern of Jurassic sea-level changes and their possible causes in the light of current knowledge. Palaeogeogr Palaeoclimatol Palaeoecol 167:23–37

Hancock PL (1985) Brittle microtectonics: principles and practice. J Struct Geol 7:437–457

Hancock PL (1994) From joints to paleostresses. In: Roure F (ed) Peri-Tethyan platforms. Editions Technip, París, pp 145–158

Haq BU, Hardenbol J, Vail PR (1988) Mesozoic and Cenozoic chronostratigraphy and cycles of sea level change. In: Wilgus CK, Hastings BS, Kendall CGStC, Posamentier HW, Ross CA, van Wagoner JC (eds) Sea-level changes—an integrated approach. SEPM Spec Publ 42:71–108

Hardenbol J, Thierry J, Farley MB, Jacquin T, De Graciansky PC, Vail PR (1998) Jurassic sequence chronostratigraphy. In: De Graciansky PC, Hardenbol J, Jacquin T, Vail PR (eds) Mesozoic and Cenozoic sequence stratigraphy of European basins. SEPM Spec Publ 60: charts 1 and 6

Haskin MA, Haskin LA (1966) Rare earths in European shales: a redetermination. Science 154:507–509

Hautvelle Y, Michels R, Malartre F, Troullier A (2006) Vascular plant biomarkers as proxies for palaeoflora and palaeoclimatic changes at the Dogger/Malm transition of the Paris Basin (France). Organic Geochem 37:610–625

Huber B, Müller B, Luterbacher H (1987) Mikropaläontologische Untersuchungen an der Callovien/Oxfordien-Grenze im Schweizer Jura und auf der Schwäbischen Alb (vorläufige Mitteilung). Eclogae Geol Helv 80:449–459

Jacquin T, de Graciansky PC (1998) Major transgressive/regressive cycles: the stratigraphic signature of European Basin development. In: de Graciansky PC, Hardenbol, J, Jacquin T, Vail PR (eds) Mesozoic and Cenozoic sequence stratigraphy of European Basins. SEPM Spec Publ 60:15–27

Jacquin T, Dardeau G, Durlet C, de Graciansky PC, Hantzpergue P (1998) The North Sea-Cycle of 2nd-order transgressive/regressive facies cycles in Western Europe. In: de Graciansky PC, Hardenbol J, Jacquin T, Vail PR (eds) Mesozoic and Cenozoic sequence stratigraphy of European Basins. SEPM Spec Publ 60:445–466

Jiménez-Espinosa R, Jiménez-Millán J, Nieto LM (1997) Factors controlling the genesis of Fe-Mn crusts in stratigraphic breaks of the eastern Betic Cordillera (SE Spain) deduced from numerical analysis of geological data. Sediment Geol 114:97–107

Jiménez-Millán J, Nieto LM (2008) Geochemical and mineralogical evidence of tectonic and sedimentary factors controlling the origin of ferromanganese crusts associated to stratigraphic discontinuities (Betic Cordilleras, SE of Spain). Chemie Erde 68:323–336

Kadiri KE (2002) Jurassic ferruginous hardgrounds of the "Dorsale Calcaire" and the Jbel Moussa Group (Internal Rif, Morocco): stratigraphical context and paleoceanographic consequences of mineralization processes. Geol Romana 36:33–69

Lécuyer C, Picard S, Garcia JP, Sheppard SMF, Grandjean P, Dromart G (2003) Thermal evolution of Tethyan surface waters during the Middle-Late Jurassic: evidence from 180 values of marine fish teeth. Palaeoceanography 18:1076

Leinfelder RR (1993) A sequence stratigraphic approach to the Upper Jurassic mixed carbonate–siliciclastic succession of the central Lusitanian Basin, Portugal. Profil 5:119–140

Leinfelder RR, Schmid DU, Nose M, Werner W (2002) Jurassic reef patterns; the expression of a changing globe. In: Kiessling W, Flügel E, Golonka J, (eds) Phanerozoic reef patterns. SEPM Spec Publ 72:465–520

Lorin S, Courville P, Collin PY, Thierry J, Tort A (2004) Modalités de réinstallation d'une plate-forme carbonatée après une crise sédimentaire: exemple de la limite Oxfordien moyen–Oxfordien supérieur dans le Sud-Est du Bassin de Paris. Bull Soc Géol France 175:289–302

Louis-Schmid B, Rais P, Bernasconi SM, Pellenard P, Collin PY, Weissert H (2007) Detailed record of the mid-Oxfordian (Late Jurassic) positive carbon-isotope excursion in two hemipelagic sections (France and Switzerland): A plate tectonic trigger? Palaeogeogr Palaeoclimatol Palaeoecol 248:459–472

Marques B, Olóriz F, Rodríguez-Tovar FJ (1991) Interactions between tectonics and eustasy during the upper Jurassic and lowermost Cretaceous. Examples from the south of Iberia. Bull Soc Géol France 126:1109–1124

Martín-Algarra A, Sánchez-Navas A (1995) Phosphate stromatolites from condensed cephalopod limestones, Upper Jurassic, Southern Spain. Sedimentology 42:893–919

Martín-Algarra A, Sánchez-Navas A (2000) Bacterially mediated authigenesis in Mesozoic stromatolites from condensed pelagic sediments (Betic Cordillera, Southern Spain). In: Glenn CR, Lucas J, Prévôt-Lucas L (eds) Marine authigenesis: from global to microbial. SEPM Spec Publ 66:499–525

Martín-Algarra A, Vera JA (1994) Mesozoic pelagic phosphate stromatolites from the Penibetic (Betic Cordillera Southern Spain). In: Bertrand-Sarfati J, Monty C (eds) Phanerozoic stromatolites II. Kluwer Academic Publishers, Dordrecht, pp 345–391

Martire L (1992) Sequence stratigraphy and condensed pelagic sediments. An example from the Rosso Ammonitico Veronese, northeastern Italy. Palaeogeogr Palaeoclimatol Palaeoecol 94:169–191

Martire L, Pavia G (2004) Jurassic sedimentary and tectonic processes at Montagna Grande (Trapanese Domain, Western Sicily, Italy). Riv Ital Paleont Stratigr 110:23–33

McEachern JA, Pemberton SG, Gingras MK, Bann KL (2007) The ichnofacies paradigm: a fifty-year retrospective. In: Miller W (ed) Trace fossils: concepts, problems, prospects. Elsevier, Amsterdam, pp 52–77

Meléndez G, Ramajo J, Martínez-Cotanda S (2005) El desarrollo de la Capa de Arroyofrío (límite Calloviense-Oxfordiense) al Sur de Zaragoza, entre Ricla y Aguilón: bioestratigrafía y facies. Geogaceta 38:3–6

Molina JM (1987) Análisis de facies del Mesozoico en el Subbético Externo (Provincia de Córdoba y Sur de Jaén). PhD Thesis, Universidad Granada, p 518

Molina JM, Ruiz-Ortiz PA, Vera JA (1995) Neptunian dykes and associated features in southern Spain: mechanics of formation and tectonic implications. Sedimentology 42:957–969

Molina JM, Ruiz-Ortiz PA, Vera JA (1999) A review of polyphase karstification in extensional tectonic regimes: Jurassic and Cretaceous examples, Betic Cordillera, southern Spain. Sediment Geol 129:71–84

Monty C (1984) Cavity and fissure dwelling stromatolites (endostromatolites) from Belgian Devonian mud mounds. Ann Soc Géol Belg 105:343–344

Nieto LM (1997). La cuenca subbética mesozoica en el sector oriental de las Cordilleras Béticas. PhD Thesis, Universidad Granada, p 556

Nieto LM, Rey J (2004) Magnitude of lateral displacement on the Crevillente Fault Zone (Betic Cordillera, SE Spain): stratigraphical and sedimentological considerations. Geol J 39:95–110

O'Dogherty L, Sandoval J, Vera JA (2000) Ammonite faunal turnover tracing sea-level changes during the Jurassic (Betic Cordillera, southern Spain). J Geol Soc Lond 157:723–736

Ogg JG (2004) The Jurassic Period. In: Gradstein FM, Ogg JG, Smith AG (eds) A geologic time scale 2004. Cambridge University Press, Cambridge, pp 307–343

Olóriz F (1978) Kimmeridgiense-Tithonico inferior en el Sector Central de las Cordilleras Béticas. Zona Subbética. PhD Thesis, Universidad Granada, p 758

Olóriz F (1979) El Kimmeridgiense en la Zona Subbética. Cuad Geol 10:475–488

Olóriz F, Reolid M, Rodríguez-Tovar FJ (2002) Fossil assemblages, lithofacies and taphofacies for interpreting depositional dynamics in epicontinental Oxfordian (Prebetic Zone, Betic Cordillera, southern Spain). Palaeogeogr Palaeoclimatol Palaeoecol 185:53–75

Olóriz F, Reolid M, Rodríguez-Tovar FJ (2004) Taphonomy of ammonite assemblages from the Middle-Upper Oxfordian (Transversarium?-Bifurcatus zones) in the Internal Prebetic (Betic Cordillera, Southern Spain): Taphonomic populations and taphofacies for ecostratigraphic interpretations. Riv Ital Paleont Stratigr 110:239–248

Olóriz F, Reolid M, Rodríguez-Tovar FJ (2008) Taphonomy of fossil macroinvertebrate assemblages for improving ecostratigraphy: Shifting eco-sedimentary conditions from carbonate to carbonate-siliciclastic shelf during the early Late Jurassic (Prebetic Zone, southern Spain). Geobios 41:31–42

Pellenard P, Deconinck JF, Marchand D, Thierry J, Fortwengler D, Vigneron G (1999) Contrôle géodynamique de la sedimentation argileuse du Callovien-Oxfordien moyen dans l'Est du Bassin de Paris: influence eustatique et volcanique. C R Acad Sci Paris 328:807–813

Pemberton SG, Frey RW, Ranger MJ, McEachern J (1992) The conceptual frame of ichnology. In: Pemberton SG (ed) Application of ichnology to petroleum exploration. SEPM Core Workshop 17:1–31

Platt JP, Allerton S, Kirker A, Mandeville C, Mayfield A, Platzman ES, Rimi A (2003) The ultimate arc: differential displacement, oroclinal bending, and vertical axis rotation in the external Betic-Rif arc. Tectonics 22:1017. doi:10.1029/2001TC001321

Platzman E, Lowrie W (1992) Palaeomagnetic evidence for rotation of the Iberian Peninsula and the external Betic Cordillera, southern Spain. Earth Planet Sci Lett 108:45–60

Podhala OG, Mutterlose J, Veizer J (1998) Preservation of $\delta^{18}O$ and $\delta^{13}C$ in belemnite rostra from the Jurassic/Early Cretaceous successions. Am J Sci 298:324–347

Price GD, Gröcke DR (2002) Strontium-isotope stratigraphy and oxygen- and carbon-isotope variation during the Middle Jurassic-early Cretaceous of the Falkland Plateau, South Atlantic. Palaeogeogr Palaeoclimatol Palaeoecol 183:209–222

Price GD, Rogov MA (2009) An isotopic appraisal of the Late Jurassic greeenhouse phase in the Russian Platform. Palaeogeogr Palaeoclimatol Palaeoecol 273:41–49

Rais P, Louis B, Bernasconi S, Weissert H (2005) Evidence for changes in intermediate-currents in the Alpine Tethys during the Late Jurassic, EGU05. Geophys Res Abstr 7:06583

Rais P, Louis-Schmid B, Bernasconi SM, Weissert H (2007) Palaeoceanographic and palaeoclimatic reorganization around the middle—late Jurassic transition. Palaeogeogr Palaeoclimatol Palaeoecol 251:527–546

Ramajo J, Aurell M (1997) Análisis sedimentológico de las discontinuidades y depósitos del Calloviense superior-Oxfordiense medio en la Cordillera Ibérica Noroccidental. Cuad Geol Ibérica 22:213–236

Ramajo J, Aurell M (2008) Long-term Callovian–Oxfordian sea-level changes and sedimentation in the Iberian carbonate platform (Jurassic, Spain): possible eustatic implications. Basin Res 20:163–184

Ramajo J, Aurell M, Cepría J (2002) Análisis de facies de la Capa de oolitos ferruginosos de Arroyofrío en la Sierra de Arcos (Jurásico, Cordillera Ibérica septentrional). J Iber Geol 28:45–64

Reolid M, Molina JM (2010) Serpulid-*Frutexites* assemblage from shadow-cryptic environments in Jurassic marine caves (Betic Cordillera, South Spain). Palaios 25:468–474

Reolid M, Nieto LM (2010) Jurassic Fe-Mn macro-oncoids from pelagic swells of the external Subbetic (Spain): evidences of microbial origin. Geol Acta 8:151–168

Reolid M, Nieto LM, Rey J (2010) Taphonomy of cephalopod assemblages from Middle Jurassic hardgrounds of pelagic swells (South Iberian Palaeomargin, Western Tethys). Palaeogeogr Palaeoclimatol Palaeoecol 292:257–271

Reolid M, El KadiriK, Abad I, Olóriz F, Jiménez-Millán J (2011) Jurassic microbial communities in hydrothermal manganese crust from the Rifian Calcareous Chain, northern Morocco. Sediment Geol 233:159–172

Rey J (1993) Análisis de la cuenca subbética durante el Jurásico y el Cretácico en la transversal Caravaca-Vélez Rubio. PhD Thesis, Universidad Granada, p 460

Ruiz-Ortiz PA, Nieto LM, Castro JM, Molina JM, Rey J (1997) Discontinuidades mayores y otros eventos jurásicos en el Subbético Externo. Correlación con otros dominios de las Cordilleras Béticas. Sur de España. Mem I Congr Latinoamericano Sediment II:239–248

Salas R, Guimerà J, Mas R, Martín-Closas C, Meléndez A, Alonso A (2001) Evolution of the Mesozoic Central Iberian Rift System and its Cainozoic inversion (Iberian Chain). In: Ziegler PA, Cavazza W, Robertson AHF, Crasquin-Soleau S (eds) Peri-Tethys Memoir 6, Peri-Tethyan Rift/Wrench basins and passive margins. Mém Mus Nat Hist Nat Sér C Sci Terre 186:145–186

Sandoval J (1979) El Bajociense de la Zona Subbética. Cuad Geol 10:425–440

Sandoval J (1983) Bioestratigrafía y paleontología (Stephanocerataceae y Perisphinctaceae) del Bajocense y Bathonense en las Cordilleras Béticas. PhD Thesis, Universidad Granada, p 613

Scouflaire Q, Marchand D, Bonnot A, Courville P, Raffray M, Huault V (1997) Le contact Callovien-Oxfordien dans les environs de Chaignay: nouvelles données stratigraphiques et paléontologiques. Bull Sci Bourgogne 49:45–63

Sequeiros L (1974) Paleobiogeografía del Calloviense y el Oxfordiense en el sector central de la Zona Subbética. PhD Thesis, Universidad Granada, p 262

Sequeiros L (1979) El Calloviense en la Zona Subbética. Cuad Geol 10:453–462

Sequeiros L, Olóriz F (1979) El Oxfordense en la Zona Subbética. Cuad Geol 10:463–474

Seyfried H (1978) Der Subbetische Jura von Murcia (Südost–Spanien). Geol Jb 29:3–204

Soussi M, M′rabet A (1991) Les faciès à oolithes ferrugineuses (‘oolitic ironstones’) du Jurassique moyen de l’Axe Nord-Sud (Tunisie centrale): caractéristiques et significations. Notes Serv Géol Tunisie 57:71–85

Stampfli GM, Borel GD (2002) A plate tectonic model for the Paleozoic and Mesozoic constrained by dynamic plate boundaries and restored synthetic oceanic isochrons. Earth Planet Sci Lett 196:17–33

Svarda CE, Bottjer DJ (1988) Limestone concretion growth documented by trace-fossil relations. Geology 16:908–911

Vera JA (1988) Evolución de los sistemas de depósito en el margen ibérico de las Cordilleras Béticas. Rev Soc Geol España 1:373–391

Vera JA (2001) Evolution of the Iberian Continental Margin. Mém Mus Nat Hist Nat Paris 186:109–143

Vera JA, Martín-Algarra A (1994) Mesozoic stratigraphic breaks and pelagic stromatolites in the Betic Cordillera (Southern Spain). In: Bertrand-Sarfati J, Monty C (eds) Phanerozoic stromatolites II. Kluwer Academic Publishers, Dordrecht, pp 319–344

Vera JA, Molina JM, Ruiz-Ortiz PA (1984) Discontinuidades estratigráficas, diques neptúnicos y brechas sinsedimentarias en la Sierra de Cabra (Mesozoico, Subbético Externo). Publ Geol Univ Autón Barcelona 20:141–162

Vera JA, Molina JM, Montero P, Bea F (1997) Jurassic guyots in the Southern Iberian Continental Margin: a model of isolated carbonate platforms on volcanic submarine edifices. Terra Nova 9:163–166

Vera JA, Martín-Algarra A, Sánchez-Gómez M, Fornós JJ, Gelabert B (2004) Cordillera Bética y Baleares. In: Vera JA (ed) Geología de España. SGE-IGME, Madrid, pp 347–464

Ziegler PA (1989) Evolution of the North Atlantic–an overview. In: Tankard AJ, Balkwill HR (eds) Extensional tectonics and stratigraphy of the North Atlantic margins. Am Assoc Petrol Geol Mem 46:111–129